Implication of the dark axion portal for the EDM of fermions and dark matter probing with NA64*e*, NA64μ, LDMX, M^3, and *BABAR*

Alexey S. Zhevlakov,[1,2,*] Dmitry V. Kirpichnikov,[3,†] and Valery E. Lyubovitskij[4,5,6,7,8,‡]

[1]*Bogoliubov Laboratory of Theoretical Physics, JINR, 141980 Dubna, Russia*
[2]*Matrosov Institute for System Dynamics and Control Theory SB RAS 134 Lermontov Street, 664033, Irkutsk, Russia*
[3]*Institute for Nuclear Research of the Russian Academy of Sciences, 117312 Moscow, Russia*
[4]*Institut für Theoretische Physik, Universität Tübingen, Kepler Center for Astro and Particle Physics, Auf der Morgenstelle 14, D-72076 Tübingen, Germany*
[5]*Departamento de Física y Centro Científico Tecnológico de Valparaíso-CCTVal, Universidad Técnica Federico Santa María, Casilla 110-V, Valparaíso, Chile*
[6]*Millennium Institute for Subatomic Physics at the High-Energy Frontier (SAPHIR) of ANID, Fernández Concha 700, Santiago, Chile*
[7]*Department of Physics, Tomsk State University, 634050 Tomsk, Russia*
[8]*Tomsk Polytechnic University, 634050 Tomsk, Russia*

(Received 22 April 2022; accepted 26 July 2022; published 17 August 2022)

The link between ordinary Standard Model (SM) photons and both dark photons and axion-like particles (ALPs) can be introduced through the dark axion portal coupling. Given the dark axion portal setup, in the present paper we refer to the dark photon as the mediator between SM and dark matter (DM) particles, implying that it decays predominantly into a pair of DM fermions. Furthermore, we discuss in detail the implication of the dark axion portal scenario for the lepton (electron and muon) fixed-target experiments. In particular, for the specific fixed-target facility we study the missing-energy signatures of the dark photon production followed by its invisible decay into stable DM particles. We investigate the potential to probe dark axion portal vertices with regarding signatures and derive the expected sensitivities of NA64*e*, NA64μ, LDMX and M^3. Moreover, we estimate the expected reach of NA64*e* from the projected statistics of the J/ψ vector meson invisible decays. We also recast the *BABAR* monophoton bounds for the specific dark axion portal scenario. In addition, we modify the dark axion portal setup by including in the model both the hadron- and lepton-specific ALP couplings. As a result, we obtain the bounds on the combination of fermion-specific couplings of ALP from the fixed-target experiments. We discuss the implication of the modified dark axion portal scenario for the electric dipole moments (EDMs) of SM fermions. In addition, we derive novel constraints on the combination of the *CP*-violating neutron-specific ALP couplings from the existing bounds on neutron EDMs by taking into account the neutron anomalous magnetic moment.

DOI: 10.1103/PhysRevD.106.035018

I. INTRODUCTION

Axion and axion-like particles (ALPs) arise naturally in the Standard Model (SM) extensions, which are connected with the *CP* violation problem in strong interaction physics [1,2], can explain the muon $(g-2)$ anomaly [3,4] and dark matter (DM) abundance [5–7]. More exotic cases of ALP phenomenology that include lepton flavor violation effects are studied in the literature thoroughly [8–11]. The ALPs and other dark sector particles have been extensively discussed recently in the context of experimental searches (see, e.g., Refs. [12–38] and references therein).

The link between SM and dark sector particles can be established through the idea of *portals* [39]. For instance, that concept includes such scenarios as the Higgs portal [40], the dark photon portal [41–43], the sterile neutrino portal [44], and the axion portal [45]. These portals offer systematic examination of the DM and also give rise to novel experimental signatures.

Recently, a new *dark axion portal* was suggested [46,47] to provide the dark photon production mechanism in the early Universe, implying an explanation of DM abundance due to the sufficiently light dark photon. Such a portal

*zhevlakov@theor.jinr.ru
†kirpich@ms2.inr.ac.ru
‡valeri.lyubovitskij@uni-tuebingen.de

Published by the American Physical Society under the terms of the Creative Commons Attribution 4.0 International license. Further distribution of this work must maintain attribution to the author(s) and the published article's title, journal citation, and DOI. Funded by SCOAP^3.

connects the axion or ALP and the dark photon via both axion–SM photon–dark photon and axion–dark photon–dark photon couplings.

Now, let us briefly summarize recent progress in the dark axion portal. In particular, the authors of Ref. [48] have developed the idea of a dark axion portal in order to explain the DM cosmic density through the mixture of both axions and dark photons. In addition, in Ref. [49], authors discussed in detail the implication of the relevant portal for the leptonic $(g-2)$ anomalies, B-factories, fixed-target neutrino experiments, and beam dumps. Also, there has been previous study [50] of the monophoton signal for the future experiments SHIP [51] and FASER [52] in the framework of a dark axion portal. Moreover, a detailed analysis of the regarding monophoton signatures and the expected sensitivities of reactor neutrino experiments was presented in Ref. [53]. The authors of Ref. [54] suggested a scenario that provides a novel link between the phenomenological dark axion portal, dark photons, and the hierarchy problem of the Higgs mass. In addition, Ref. [55] proposed a new scenario of using the dark axion portal at the one-loop level in order to explain the recent results of the Fermilab muon $(g-2)$ experiment on the muon anomalous magnetic moment.

In the first part of this paper, we develop the ideas presented in Refs. [56,57], where the implications of light sub-GeV bosons for the electric dipole moments (EDMs) of fermions and the CP-odd dark axion portal coupling were discussed in detail. In particular, we study the contribution of CP-violation vertices of SM fermions and ALPs to EDM and derive a novel constraint on the combination of couplings of neutrons with ALPs. In addition, we argue that the EDM of fermions can be induced by (i) CP-odd Yukawa-like couplings of ALP, (ii) CP-even interactions of SM fermions and dark photons, and (iii) CP-even dark axion portal coupling. As a result, one can obtain the bounds on the combination of regarding couplings.

The second part of the paper develops the idea suggested in Refs. [49,50] that implies probing the dark ALP portal scenario through the dark photon decaying predominantly to the DM particles. In this setup, it is assumed that the dark photon is the gauge field of the hidden $U_D(1)$ group, and thus it can serve the mediator between DM and SM particles via dark axion portal interaction. We show that the regarding scenario has a very broad phenomenological implication and can be probed via missing-energy signatures in the existent (NA64e [31–35] and NA64μ [58–61]) and the projected (LDMX [62–67] and M^3 [68,69]) lepton fixed-target facilities. We also recast the *BABAR* constraints on the dark ALP portal scenario with dark photons decaying mainly to DM fermion pairs. In addition, we address the CP-violating interaction of ALP with SM fermions in order to modify the dark ALP portal scenario; as a result, we obtain the expected bounds on the combination of hadron-specific and lepton-specific couplings from NA64e, NA64μ, LDMX, and M^3.

The paper is organized as follows: In Sec. II, we provide a description of the considered modified dark ALP portal scenarios. In Sec. III, we consider dark ALP portals applied to the generation of EDM. In Sec. IV, we give a description of the missing-energy signatures for the analysis of dark matter production at the fixed-target experiments. In Sec. V, we show that dark ALP portal couplings can be constrained by using the data from e^+e^- colliders and experiments that exploit the electron and muon beam impinging on the fixed target. In Secs. VI and VII, we obtain the constraints on the combination of dark axion portal coupling with both hadron-specific and lepton-specific interactions, respectively. In Sec. VIII, we summarize our main results.

II. DESCRIPTION OF THE BENCHMARK SCENARIOS

One of the possible connections between SM and dark sector particles is a vector portal via the coupling of the SM and dark photons. One can describe this mixing by using the effective phenomenological Lagrangian

$$\mathcal{L}_{\text{vector portal}} = \frac{\epsilon}{2} F_{\mu\nu} F'^{\mu\nu}, \tag{1}$$

where ϵ is the kinetic mixing parameter between the two $U(1)$ gauge symmetries [70], and $F_{\mu\nu}$ and $F'_{\mu\nu}$ are the strength tensors of SM electromagnetic and DM dark gauge (dark photon) fields, respectively. Nevertheless, in the present analysis, we assume throughout the paper that $\epsilon \ll 1$, implying that we are completely neglecting the vector portal mixing in Eq. (1).

In what follows, one can assume [46,47] that mixing between dark and electromagnetic photons can be associated with ALP interaction. The effective Lagrangian for such a nonrenormalizable dark axion portal has the form

$$\mathcal{L}_{\text{dark axion portal}} = \frac{g_{a\gamma_D\gamma_D}}{4} a F'_{\mu\nu} \tilde{F}'^{\mu\nu} + \frac{g_{a\gamma\gamma_D}}{2} a F_{\mu\nu} \tilde{F}'^{\mu\nu}, \tag{2}$$

where the first term is the coupling between an ALP and two dark photons, and the second term is the interaction between an ALP and both a SM and a dark photon.

First, we consider the benchmark extension of the dark axion portal setup by exploiting the dark matter (DM) Lagrangian, such that the dark photon serves as the mediator between the visible SM photon and hidden DM sectors through the Lagrangian in Eq. (2). In particular, we specify throughout the paper the Lagrangian

$$\mathcal{L} \supset \mathcal{L}_{\text{dark axion portal}} + \bar{\chi}(\gamma^\mu i\partial_\mu - g_D \gamma^\mu A'_\mu + m_\chi)\chi, \tag{3}$$

which is referred to as the *minimal dark ALP portal scenario*.

The field χ in Eq. (3) is a Dirac DM fermion of mass m_χ from the dark sector, where g_D is the coupling constant between the DM and dark photon A'_μ field, which is

associated with the hidden charge of the $U_D(1)$ gauge group. Moreover, we assume that a dark photon decays predominantly to a dark fermion $\chi\bar{\chi}$ pair.

Second, we also employ a simplified model framework, with a *CP*-violation Yukawa coupling between ALP and SM fermions that can be written as

$$\mathcal{L} \supset \mathcal{L}_{\text{dark axion portal}} + \bar{\chi}(\gamma^\mu i\partial_\mu - g_D\gamma^\mu A'_\mu + m_\chi)\chi + \sum_\psi a\bar{\psi}(g^s_\psi + ig^p_\psi\gamma_5)\psi, \tag{4}$$

where the couplings, g^s_ψ and g^a_ψ, are restricted to be from two benchmark scenarios:

(1) The *nonminimal lepton-specific ALP setup*: $g^s_\psi \neq 0$, $g^p_\psi \neq 0$ for $\psi = e, \mu$, where e and μ are the electron and muon, respectively, and $g^s_\psi = g^p_\psi = 0$ for $\psi = n$, p, where p and n are the proton and neutron, respectively.

(2) The *nonminimal hadron-specific ALP setup*: $g^s_\psi \neq 0$, $g^p_\psi \neq 0$ for $\psi = n$, p and $g^s_\psi = g^p_\psi = 0$ for $\psi = e, \mu$.

The Yukawa-like couplings of the Lagrangian in Eq. (4) may originate from an effective interaction [71–74] in the framework of the two-Higgs-doublet model. Moreover, since such terms violate the *CP* symmetry, they can induce the electric dipole moment (EDM) [75,76] of fermions. It is worth estimating the bounds on the regarding couplings from the EDMs of fermions in the framework of both the lepton-specific and hadron-specific scenarios. That study is of particular interest to the present paper. In Sec. III, we discuss its phenomenological implications.

In addition, for the specific benchmark scenario, one can also obtain the upper limit/expected sensitivity on either the coupling $g_{a\gamma\gamma_D}$ or the combination of couplings $|g_{a\gamma\gamma_D} g^s_\psi|$ and $|g_{a\gamma\gamma_D} g^p_\psi|$ from the null result of DM detection in the *BABAR* e^+e^- collider and in fixed-target experiments such as NA64$e(\mu)$ at CERN SPS and LDMX at SLAC M^3 at FermiLab. We discuss this in detail in Secs. IV, V, VI, and VII.

III. EDM

Let us consider the bounds on ALP couplings from the experimental constraints on EDM fermions (electrons, muons, and neutrons) generated by a *CP*-violating Lagrangian [77,78]. We can estimate a contribution to EDM by calculation using simple Feynman diagrams (see Fig. 1) with intermediate ALP exchange [56]. The contribution to the fermion EDM with mass m_ψ has the form

$$d_\psi = \frac{e g^s_\psi g^p_\psi}{8\pi^2 m_\psi} g_i(y), \tag{5}$$

where the index $i = 1$ labels the lepton couplings ($\psi = e$, μ), with the function $g_1(y)$ being

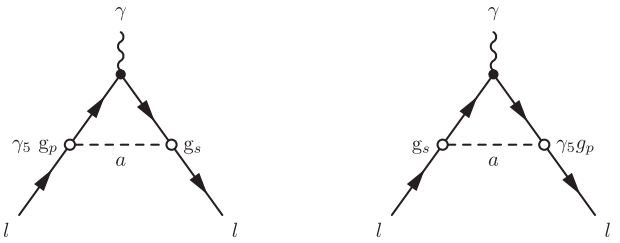

FIG. 1. Feynman diagrams taking into account ALPs, which generate an EDM of charge fermions, leptons.

$$g_1(y) = \int_0^1 dx \frac{x^2}{x^2 + y^2(1-x)}, \tag{6}$$

here $y = m_a/m_\psi$. For the neutron case ($\psi = n$), we specify the index $i = 2$ in Eq. (5). Then, one should account for the neutron interaction with the external electromagnetic field A_μ through the anomalous magnetic moment (see diagrams in Fig. 2). The regarding Lagrangian can be written in the following form:

$$\mathcal{L}_{ANN} = ieA_\mu \bar{N}\left(\gamma^\mu Q_N + \frac{i\sigma^{\mu\nu}q_\nu}{2m_N}k_N\right)N, \tag{7}$$

where m_N is the nucleon mass, and $Q_N = \text{diag}(1, 0)$ and $k_N = \text{diag}(k_p, k_n)$ are the matrices of the electric charges and the anomalous magnetic moments of nucleons (proton p and neutron n), respectively, with $k_p = 1.793$ and $k_n = -1.913$. Here, $\sigma^{\mu\nu} = \frac{i}{2}[\gamma^\mu, \gamma^\nu]$, where γ^α are Dirac gamma matrices. Using the magnetic moment of the neutron, we can calculate its contribution to the EDM generated by ALP exchange at the one-loop level [see, e.g., Eq. (5) and Fig. 2 for details], the regarding $g_2(y)$ structure of the Feynman integral can be written as

$$g_2(y) = k_n \int_0^1 dx \frac{(1-x)(1-x^2)}{(1-x)^2 + y^2 x}, \tag{8}$$

where $y = m_a/m_N$. Besides dark ALPs scenario can generate EDM from diagrams which presented on Fig. 3

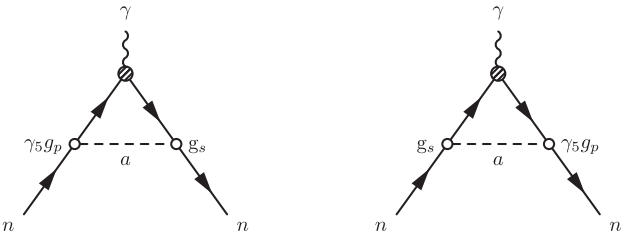

FIG. 2. Feynman diagrams, taking into account ALPs which generate neutron EDMs induced by nonminimal electromagnetic couplings (anomalous magnetic moments) with an external electromagnetic field (shaded blob).

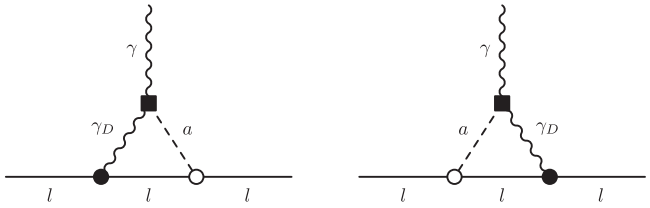

FIG. 3. Feynman diagrams which generate EDM terms due to axions coupled with both dark and SM photons [see, e.g., Eq. (10) for details].

and will be briefly discussed later. The analytic expression for the loop integrals $g_i(y)$ is presented in Appendix A.

The boundaries for the combination of couplings $|g_s^\psi g_p^\psi|$ [57,75] as a function of the ALP mass m_a are shown in Fig. 4. The difference in behavior of different boundaries is connected with the mass of fermions and existing limits to their EDMs ($|d_e| < 1.1 \times 10^{-29}\mathrm{e}\cdot\mathrm{cm}$, $|d_\mu| < 1.8 \times 10^{-19}\mathrm{e}\cdot\mathrm{cm}$, and $|d_n| < 1.8 \times 10^{-26}\mathrm{e}\cdot\mathrm{cm}$; see Ref. [79] from the Particle Data Group). Bounds on $|g_s^n g_p^n|$ from the neutron EDM for light masses of ALPs are proportional to $\bar{\theta}$, a parameter of CP violation of the vacuum in quantum chromodynamics (QCD) whose typical value is $\sim 10^{-10}$ [80,81]. It is a general neutron EDM feature due to the light scalar/pseudoscalar boson exchange in one loop [81] or two loops with the CP-violation vertex [80,82–84].

However, from the EDM of fermions we can estimate only the combination of ALPs couplings g_s^ψ and g_p^ψ, wherein we want to note that the Lagrangian with universal CP-violating couplings to the SM fermions,

$$\mathcal{L}_{\not CP} \supset \sum_\psi \bar{\psi}\, a(g_\psi^s + i g_\psi^p \gamma_5)\psi, \tag{9}$$

plays an important role in spin interaction. In particular, by exploiting the data on Schiff moments of atoms or molecules,

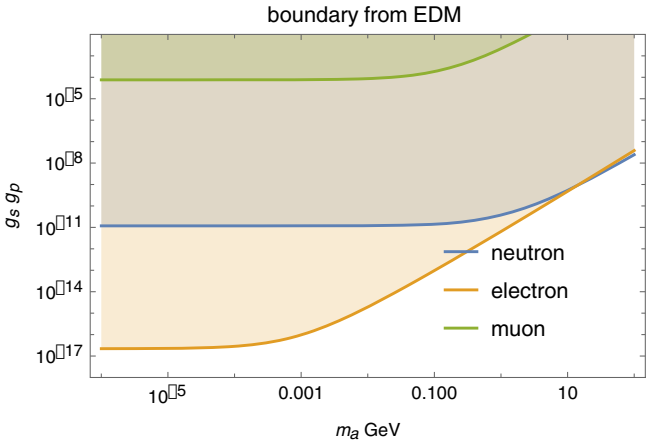

FIG. 4. Boundaries for the product of scalar and pseudoscalar couplings from an EDM neutron and electron/muon as a function of the ALP mass. These boundaries correspond to leptophilic and hadrophilic scenarios.

it is straightforward to constrain the combination of couplings $|g_N^s g_e^p|$ (see, e.g., Refs. [75,78,85] for details).

We would like to stress that the ALPs in the considered scenario could contribute to the fermion EDMs. The corresponding matrix element is induced by the CP-violating diagrams analogous to the Barr-Zee diagrams with ALP exchange in the loop (see Fig. 3). This contribution is generated by an additional interaction Lagrangian containing three terms: (i) the P-parity-violating coupling of ALPs with SM fermions, (ii) the P-parity-conserving coupling of ALPs with SM photons and dark photons, and (iii) the P-parity-conserving coupling of dark photons with SM fermions:

$$\mathcal{L} \supset a\left[g_s \bar{\psi}\psi + \frac{g_{a\gamma\gamma_D}}{2} F_{\mu\nu}\tilde{F}'^{\mu\nu}\right] + e\epsilon\bar{\psi}\gamma^\mu A'_\mu\psi. \tag{10}$$

The detailed analysis of the present bounds would require the consideration of both the vector portal and dark ALP portal scenarios. Such analysis is beyond the scope of the present paper, and we leave it for future study. In particular, we consider regarding limits elsewhere [86], just collecting some general formulas in Appendix B.

IV. THE MISSING-ENERGY SIGNAL

In this section, we discuss the setups for the fixed-target experiments such as NA64e [31–35], LDMX [62–67], NA64μ [58–61], and M^3 [68,69], which can potentially probe the invisible signatures associated with a lepton missing-energy process

$$lZ \to Zl(E_{\mathrm{miss}}), \tag{11}$$

where $l = (e, \mu)$ is the label for either the electron or muon beam and Z designates the target nucleus. For instance, in the framework of the minimal dark ALP portal scenario, the missing energy of the lepton beam E_{miss} can arise from the production of the ALP a and dark photon γ_D by the off-shell photon γ^* in the process $lZ \to lZ\gamma^* \to lZa\gamma_D(\to \bar{\chi}\chi)$

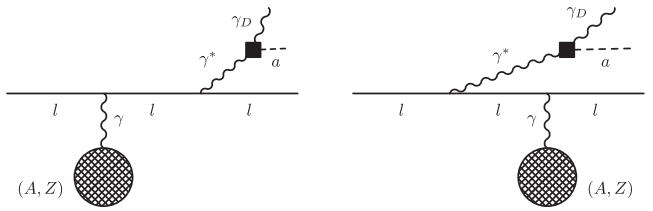

FIG. 5. Feynman diagrams for radiative ALP and dark photon production by an impinging lepton on a nucleus Z. The regarding process represents the missing-energy signature for the minimal dark ALP portal scenario $\mathcal{L} \supset \frac{1}{2} g_{a\gamma\gamma_D} a F_{\mu\nu}\tilde{F}'_{\mu\mu}$ Note that we neglect in the calculation the diagrams with off-shell photons from the nucleus leg, since their contribution to the signal process is suppressed by a factor of $(Zm_l/M_Z)^2$ for both electrons and muons impinging on the nucleus.

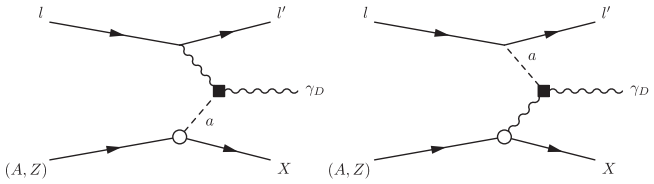

FIG. 6. Feynman diagrams for processes of the lepton scattering off an atomic target (A, Z) in which the SM and dark photon interact through the axion portal coupling for both ALP-hadrophilic (left) and ALP-leptophilic (right) scenarios.

(see, e.g., Fig. 5 for detail). To calculate the regarding yield, we use the state-of-the-art CalcHEP package [87].

In addition, for the hadron-specific and lepton-specific couplings of the ALPs, the missing-energy process $lZ \to lZ\gamma_D(\to \bar{\chi}\chi)$ is possible. This reaction implies that dark photon production is associated with the interaction of the ALP with a SM photon which is produced by either the beam or target (see, e.g., Fig. 6 for detail). To calculate the cross section of these processes, we exploit the approximation of equivalent photons, also known as the Weizsacker-Williams (WW) [88–90] approximation. This approach is common for DM production study in the beam dump and fixed-target experiments. It implies replacing the fast-moving charged particles with a specific photon distribution.

The dark photon can decay through the different channels in the dark ALP portal scenario. In particular, as soon as $m_{\gamma_D} \gtrsim m_a$, the visible two-body decay through the ALP and photon is kinetically accessible with a decay width [50]

$$\Gamma_{\gamma_D \to a\gamma} = \frac{g^2_{a\gamma\gamma_D}}{96\pi} m^3_{\gamma_D} \left(1 - \frac{m^2_a}{m^2_{\gamma_D}}\right)^3. \tag{12}$$

Lagrangian (3) implies that the invisible two-body decay of the dark photon γ_D into a $\bar{\chi}\chi$ pair is also allowed with a decay width [91]

$$\Gamma_{\gamma_D \to \bar{\chi}\chi} = \frac{g^2_D}{12\pi} m_{\gamma_D} \left(1 + \frac{2m^2_\chi}{m^2_{\gamma_D}}\right) \left(1 - \frac{4m^2_\chi}{m^2_{\gamma_D}}\right)^{1/2}. \tag{13}$$

In the present paper, we will focus on the process of the invisible channel of dark photon decay into a pair of hidden dark fermions, $\gamma_D \to \bar{\chi}\chi$ with $\mathrm{Br}(\gamma_D \to \bar{\chi}\chi) \simeq 1$ for $m_\chi \ll m_{\gamma_D}$. That implies the following condition on decay widths: $\Gamma_{\gamma_D \to \bar{\chi}\chi} \gg \Gamma_{\gamma_D \to a\gamma}$, and as a result this yields $g_D \gg g_{a\gamma\gamma_D} m_{\gamma_D}$. Therefore, it leads to the rapid decay of the dark photon into a $\bar{\chi}\chi$ pair after its production. In addition, in our analysis throughout the paper, we keep the ALP mass m_a well below m_{γ_D}, such that $m_a \ll m_{\gamma_D}$, to get rid of the possible visible decay signatures $a \to \gamma\gamma_D$ in the detector of the fixed-target facility.

To begin with, we estimate the number of missing-energy events for the lepton beam with a fixed target as follows:

$$N_{\mathrm{sign}} \simeq \mathrm{LOT} \cdot \frac{\rho N_A}{A} L_T \int_{x_{\min}}^{x_{\max}} dx \frac{d\sigma(E_l)}{dx} \mathrm{Br}(\gamma_D \to \chi\bar{\chi}), \tag{14}$$

where E_l is the initial energy of the beam, A is the atomic weight number of the target material, N_A is Avogadro's number, LOT is the number of leptons accumulated on the target, ρ is the target density, L_T is the effective thickness of the target, $d\sigma/dx$ is differential cross section for the specific missing-energy channel $lZ \to Zl(E_{\mathrm{miss}})$, and $x_{\min}$ and $x_{\max}$ are the minimal and maximal fraction of the lepton energy $x = E_{\mathrm{miss}}/E_l$ that hidden particles carry away. The cuts on x are determined by the specific fixed-target facility.

Let us discuss now the benchmark input parameters for each specific experimental setup.

A. The NA64*e* experiment

The dark photon and/or ALP can be produced in the reaction of high-energy electrons of $E_e = 100$ GeV scattering off the nuclei of an active lead ECAL target:

$$eZ \to eZ\gamma_D(a), \tag{15}$$

followed by prompt $\gamma_D \to \bar{\chi}\chi$ decay into dark matter particles (χ). Thus, the fraction $E_{\mathrm{miss}} = xE_e$ of the primary beam energy is carried away by the χ's (a), which penetrate the detector of NA64*e* without energy deposition. The remaining part of the beam energy fraction $E^{\mathrm{rec}}_e \equiv E_e(1-x)$ is deposited in the ECAL target by the scattered electrons. Therefore, the occurrence of the hidden particles produced in the process [Eq. (11)] leads to an excess of events with a single electromagnetic (EM) shower with energy E^{rec}_e above the expected background (see, e.g., Ref. [30] for detail). In the present analysis, we conservatively assume that the EM shower is localized in the first radiation length of the lead detector $X_0 = 0.56$ cm, such that the effective thickness of the target in Eq. (14) is $L_T \simeq X_0$. That implies that the dominant production of the hidden particles occurs within the first radiation length of the active ECAL target [92]. The candidate events are requested to have the missing energy in the range $E^{\mathrm{rec}}_e \lesssim 0.5E_e$, implying that $x_{\min} = 0.5$ in Eq. (14).

The ECAL target of NA64*e* is a matrix of 6×6 Shashlyk-type modules assembled from lead (Pb) ($\rho = 11.34$ g cm^{-3}, $A = 207$ g mole^{-1}, $Z = 82$) and scintillator (Sc) plates. Note that the production of hidden particles in the scintillator is subleading due to its larger radiation length, $X_0(Sc) \gg X_0(Pb)$; thus, we ignore it in the calculation.

The NA64*e* employs the optimized electron beam from the $H4$ beam line at the SPS. The maximum intensity of the beam is $\simeq 10^7$ electrons per spill of 4.8 s; the number of good spills per day is estimated to be 4000. Therefore, approximately 120 days are required to accumulate 5×10^{12} electrons on target (EOT) at the H4 electron beam line.

B. The LDMX experiments

The LDMX is the proposed fixed-target experiment at Fermilab that exploits the electron beam as well as the NA64e facility. The LDMX is designed to measure the missing momentum of the electron; thus, probing of the process in Eq. (15) at LDMX is complementary to NA64e. Moreover, the missing-momentum cuts and the active veto systems of both experiments make them essentially background free [30,63]. The proposed LDMX facility consists of a target, a silicon tracker system, and an electromagnetic and hadron calorimeter (for details, see, e.g., Refs. [63,67]). Most of the electron beam energy is lost due to the emission of the dark particles occurring in the thin upstream target. The missing momentum of the electron is tagged by the silicon tracker and the downstream electromagnetic and hadron calorimeter. The final-state electron missing-energy cut is chosen to be $E_e^{\rm rec} \lesssim 0.3E_e$, which corresponds to $x_{\rm min} = 0.7$ in Eq. (14). In our analysis, we carry out the calculation for the aluminum target (Al) ($X_0 = 8.9$ cm, $\rho = 2.7$ g cm^{-3}, $A = 27$ g mole^{-1}, $Z = 13$) with a thickness of $L_T \simeq 0.4X_0$. Note that the LDMX plans to accumulate EOT $\simeq 10^{16}$ with the beam energy up to $E_e = 16$ GeV for the final phase of running after 2027 [67].

C. The NA64μ experiment

The NA64μ facility [60,61] is a complementary experiment to the NA64e that searches for the dark sector particles in the muon beam mode:

$$\mu Z \to \mu Z \gamma_D(a). \tag{16}$$

In our calculations, we set the muon beam energy of NA64μ to be $E_\mu \simeq 160$ GeV; the muon flux is chosen to be about MOT $\simeq 5 \times 10^{13}$ for the projected statistics. We consider the lead Shashlyk-type electromagnetic calorimeter that serves a target with a typical thickness of $L_T \simeq 40X_0 \simeq 22.5$ cm. We also neglect the muon stopping loss in the lead target [93,94], since its typical energy attenuation is rather small ($\langle dE_\mu/dx\rangle \simeq 12.7 \times 10^{-3}$ GeV/cm), for the ultrarelativistic approach $E_\mu \simeq 160$ GeV.

The NA64μ facility exploits two magnet spectrometers, allowing for precise measurements of momenta for incident and outgoing muons [61]. We set a cut on the energy of the recoiling muon, $E_\mu^{\rm rec} \lesssim 0.5E_\mu \simeq 80$ GeV, so that $x_{\rm min} = 0.5$.

We also note that the intensity of 160 GeV muons at the M2 beam line can be higher by a factor of 10 than that for the electrons. Therefore, about the same running time of 120 days is required to accumulate much higher statistics of 5×10^{13} muons on target (MOT) relative to EOT $= 5 \times 10^{12}$ for NA64e.

D. The M^3 experiments

The M^3 (muon missing-momentum) experiments at Fermilab [68] are a projected modification of the LDMX facility that is suitable for probing the muon-specific missing-energy signatures, $\mu Z \to \mu Z \gamma_D(a)$. In particular, it considers new physics discovery potential for the muon beam of $E_\mu \simeq 15$ GeV with a thick tungsten target (W) ($X_0 \simeq 0.35$ cm, $\rho = 19.3$ g cm^{-3}, $A \simeq 184$ g mole^{-1}, $Z = 74$) of thickness $L_T = 50X_0 \simeq 17.5$ cm and a downstream detector to veto SM backgrounds.

The M^3 plans to accumulate 10^3 MOT within $\simeq$3 months of data taking. The signal missing-momentum signature of the recoil muon is $E_\mu^{\rm rec} \lesssim 9$ GeV, meaning that $x_{\rm min} = 0.4$ in Eq. (14). The reported [68] muon stopping loss is 530 MeV through a tungsten target of $50X_0$ for muons of $E_\mu \simeq 15$ GeV. We neglect $\langle dE/dx\rangle$ in the signal estimate for the sake of simplicity. Given that approach, one can exploit Eq. (14) for the signal yield estimate.

V. MINIMAL DARK ALP PORTAL SCENARIO

In this section, for the minimal dark ALP portal setup [Eq. (3)], we discuss the experimental signature of dark photon and ALP production in the processes

(1) $e(\mu)Z \to e(\mu)Z\gamma^* \to e(\mu)Za\gamma_D$, which is shown in Fig. 5 for the fixed-target experiments.
(2) J/ψ vector meson photoproduction, $eZ \to eZJ/\psi$ followed by invisible decay $J/\psi \to a\gamma_D$, at the NA64e experiment (see, e.g., Fig. 7 for details).
(3) $e^+e^- \to \gamma\gamma^* \to \gamma(\gamma^* \to a\gamma_D) \to \gamma a\gamma_D$, which is shown in Fig. 8 for the *BABAR* experiment.

In particular, we estimate the rates of these processes and calculate the sensitivity curves from the null result of the experimental facilities.

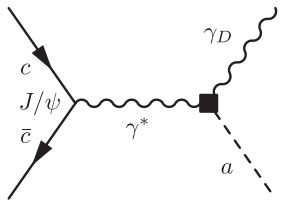

FIG. 7. Feynman diagrams for the radiative $J/\psi \to \gamma^* \to a\gamma_D$ decay.

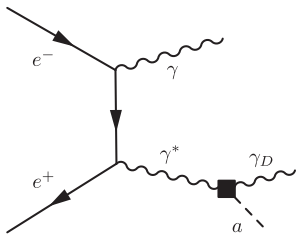

FIG. 8. Feynman diagrams for the monophoton three-body process $e^+e^- \to a\gamma\gamma_D$ followed by invisible dark photon decay into a DM fermion pair, $\gamma_D \to \chi\bar{\chi}$. That reaction is relevant for the *BABAR* constraints on $g_{a\gamma\gamma_D}$ coupling in the framework of the minimal dark ALP portal scenario.

A. Radiative cross sections of the fixed-target facilities

In order to estimate the sensitivity of the lepton fixed-target experiments to probe minimal dark ALP portal missing-energy signatures, we calculate cross sections by exploiting the state-of-the-art CalcHEP package [87]. In the SM model of CalcHEP, we add both the massive ALP a and the dark photon γ_D as new particles by including the corresponding interaction Lagrangian with the photon $\mathcal{L} \supset (1/2) g_{a\gamma\gamma_D} a F_{\mu\nu} \tilde{F}'_{\mu\nu}$. We also add a target nucleus with atomic number A, charge Z, with spin $1/2$ particle, and with mass M_Z that couples the SM photon via the $U(1)$ vertex $ieZF(t)\gamma_\mu$, where $t = -q^2 > 0$ is a nucleus transfer momentum squared, and $F(t)$ is an elastic form factor that can be written as

$$F(t) = \frac{a^2 t}{(1 + a^2 t)} \frac{1}{(1 + t/d)}. \tag{17}$$

Here, $a = 111 Z^{-1/3}/m_e$ and $d = 0.164 A^{-2/3}$ GeV^2 are the form-factor parameters of screening and nucleus size, respectively [95,96]. The form factor specified in Eq. (17) was implemented in the C++ files for the expression of the matrix element squared, $|\mathcal{M}(lZ \to lZa\gamma_D)|^2$, which is generated in the analytical session of CalcHEP.

Given the input parameters of the experiments discussed in Sec. IV, we carry out the integration of the exact tree-level amplitude squared $e(\mu)Z \to e(\mu)Za\gamma_D$ over the phase space of the outgoing particles by exploiting the CalcHEP package. In particular, for the specific chemical element of the target and typical energies of the lepton beam E_l, we calculate $\sigma_{\rm tot}$ as a function of the mass m_{γ_D} in the range 1 MeV $\lesssim m_{\gamma_D} \lesssim 1$ GeV for $m_a \simeq 10$ keV. The numerical integration was performed by the VEGAS importance sampling algorithm with $N_{session} = 10$ runs and $N_{\rm calls} = 10^6$ sampling points during each run. The grid adapting of the VEGAS algorithm was performed with a fairly good accuracy of $\mathcal{O}(0.1)\%$–$\mathcal{O}(0.01)\%$ in the numerical session of CalcHEP.

In Fig. 9, we show the differential cross sections as a function of the missing energy, $E_{\rm miss} = E_{\gamma_D} + E_a$, in the signal box range $E_l^{th} \lesssim E_{\rm miss} \lesssim E_l$ for the fixed-target experiments and various masses m_{γ_D}; here we denote $E_l^{th} = x_{\rm min} E_l$. Both the NA64$e$ and LDMX cross sections have a peak at $E_{\rm miss} \simeq E_e$, which implies that the signal is strongly forward peak for $E_{\rm miss} \gg m_{\gamma_D}, m_a$, and the

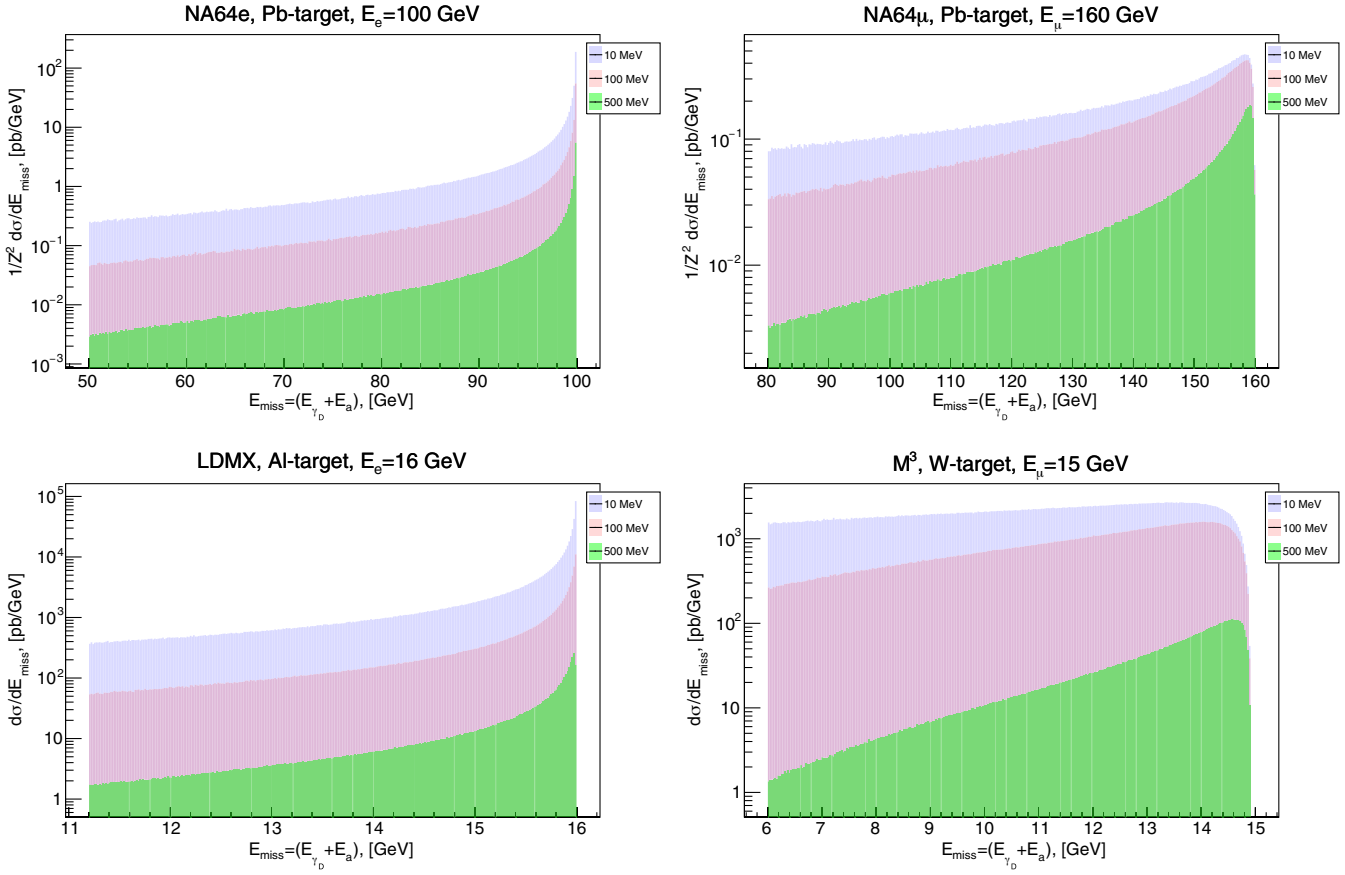

FIG. 9. The differential spectra of the process $lZ \to lZa\gamma_D(\to \chi\bar{\chi})$ as a function of the missing energy $E_{\rm miss} = E_{\gamma_D} + E_a$ for various experimental fixed-target facilities and for the set of dark photon masses $m_{\gamma_D} = 10$ MeV, $m_{\gamma_D} = 100$ MeV, and $m_{\gamma_D} = 500$ MeV in the framework of the minimal dark ALP portal scenario. We set $g_{a\gamma\gamma_D} = 1$ GeV^{-1} and $m_a = 10$ keV.

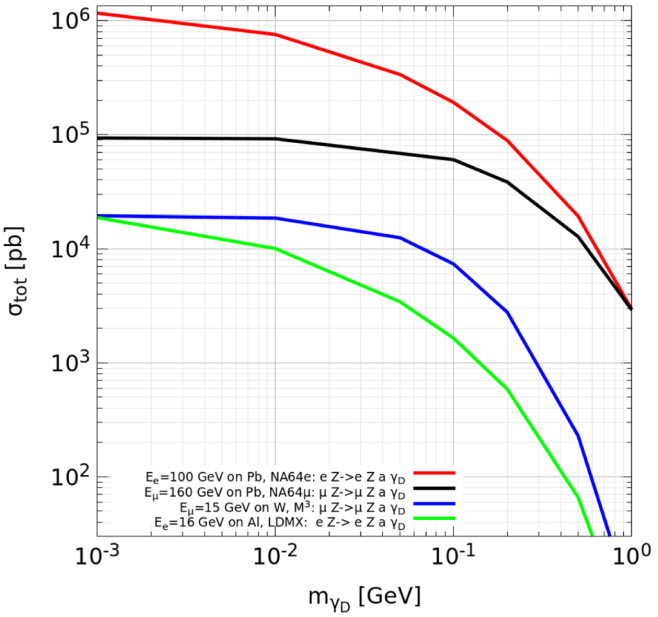

FIG. 10. The total cross section as a function of the mass m_{γ_D} for the minimal portal scenario, where $m_a \simeq 10$ keV. We set here $g_{a\gamma\gamma_D} = 1$ GeV^{-1} and integrate the cross section over the experimental cut range $x_{\min} \lesssim x \lesssim x_{\max}$. The red line is the cross section for the NA64e experiment, the black line corresponds to the NA64μ experiment, the blue line is the total cross section for the M^3 experiment, and the green line corresponds to the cross section of the LDMX facility.

dominant part of the beam energy transfers to the $a\gamma_D$ pair. However, for the muon beam cross sections of both NA64μ and M^3, the peak at $E_{\text{miss}} \lesssim E_\mu$ is mitigated, since the production rates of the $a\gamma_D$ pair are in the soft bremsstrahlung-like regime as long as $m_{\gamma_D}, m_a \lesssim m_\mu$.

In Fig. 10, the resulting total cross sections are shown for the NA64e, NA64μ, LDMX, and M^3 experimental facilities. It is worth mentioning that the NA64e cross section σ_e^{tot} in Fig. 10 for the lead (Pb) target ($Z \simeq 82$) with an impinging electron beam of $E_e = 100$ GeV is generally larger by a factor of $\simeq$10 than the lead cross section σ_μ^{tot} for the muon beam of $E_\mu = 160$ GeV. Therefore, there is a cross-section advantage of using the electron beam instead of a muon beam in the low-mass region $m_{\gamma_D} \gtrsim 1$ MeV, as long as both the electron and muon have typical energies of the order of $E_\mu \simeq E_e \simeq \mathcal{O}(100)$ GeV. On the other hand, σ_e^{tot} decreases more rapidly than σ_μ^{tot} as m_{γ_D} increases towards 1 GeV in the mass range of interest, $m_{\gamma_D} \lesssim 1$ GeV. The latter one scales as $\sigma_\mu^{\text{tot}} \propto g_{a\gamma\gamma_D}^2$ and depends weakly on m_{γ_D} for the bremsstrahlung-like regime as long as $m_a, m_{\gamma_D} \ll m_\mu$.

In addition, one can see from Fig. 10 that the LDMX cross section for the aluminum (Al) target ($Z \simeq 13$) is smaller than the cross section for the lead target of the NA64e facility, since the rate of $a\gamma_D$ production scales with $\propto Z^2$ and the aluminum nucleus charge is smaller by a factor of $82/13 \simeq 6.3$.

However, if we compare the M^3 cross section for the tungsten (W) target ($Z \simeq 74$) with an impinging muon beam of $E_\mu \simeq 15$ GeV and the LDMX cross section with impinging electrons of $E_e \simeq 16$ GeV, one can conclude that the advantage of the electron beam in the low-mass region $m_{\gamma_D} \gtrsim 1$ MeV is compensated by the nucleus charge suppression. As a result, the cross sections of M^3 and LDMX are both of the same order of magnitude at $m_{\gamma_D} \simeq 1$ MeV.

B. Limits from the fixed-target experiments

Using the formula (14) for the number of produced $a\gamma_D$ pairs and the results on the production cross sections, we find the expected bounds on the coupling $g_{a\gamma\gamma_D}$ for the minimal dark ALP portal scenario. We require $N_{\text{sign}} \gtrsim 2.3$, which corresponds to the 90% C.L. exclusion limit on the coupling $g_{a\gamma\gamma_D}$ for the background free case and null result of the fixed-target experiments. In Fig. 11, we show the expected reach of NA64e, LDMX, NA64μ, and M^3. Note that projected limits on $g_{a\gamma\gamma_D}$ from LDMX are fairly strong, even though the cross section of $a\gamma_D$ pair production at LDMX is relatively small (see, e.g., the green line in Fig. 10). The regarding LDMX sensitivity enchantment can be explained by the large number of projected accumulated statistics, EOT $\simeq 10^{16}$, by the final phase of experimental running. In addition, we note also from the M^3 and NA64μ cross section shown in Fig. 10 that the signal of $a\gamma_D$ pair production by the muon beam drops as the energy of muons decreases. In particular, compared to the M^3 option with 16 GeV beam muons, the higher energy (e.g., 160 GeV) muons of NA64μ allow for probing a wider region in the parameter space of the minimal dark ALP portal scenario for MOT $= 10^{13}$. In addition, we note that the projected limits of NA64e for EOT $\simeq 5 \times 10^{12}$ can be ruled out by other fixed-target experiments.

In Fig. 11, we show by the shaded red region the excluded limits of NA64e for the current accumulated statistics [34] of EOT $\simeq 3 \times 10^{11}$. This region rules out at 90% C.L. the typical parameter space of the minimal dark ALP portal scenario [49] that can explain the $(g-2)_\mu$ and $(g-2)_e$ anomalies [3,97–99] at the two-loop level. That contribution of the ALP and dark photon is analogous to the neutral pion term [100] that contributes the two-loop hadronic part of the charged fermion $(g-2)_f$.

Concluding this subsection, we note that there is a detector advantage of exploiting the muons at NA64μ instead of electrons at NA64e, even though both experiments have a target total equivalent thickness of $40X_0 \simeq 22.5$ cm. The key point of that idea is the following [94]: The electron beam of $E_e \simeq 100$ GeV degrades significantly within the first radiation length X_0 of the lead target. Contrarily, the muons pass the target without a significant loss of energy, since their radiation length scales as $X_0^\mu \simeq (m_\mu/m_e)^2 X_0 \gg X_0$. This implies that the missing-momentum signal of NA64μ is scaled as $N_{\text{sign}} \propto L_T$.

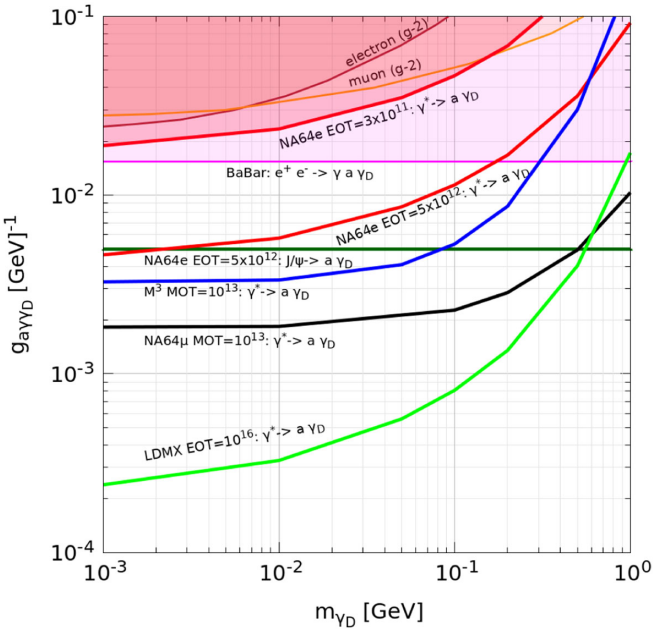

FIG. 11. The limits on $g_{a\gamma\gamma_D}$ coupling from the fixed-target experiments and *BABAR* for the minimal dark ALP portal setup as a function of the dark photon mass m_{γ_D}. For all sensitivity curves, we imply that $\mathrm{Br}(\gamma_D \to \chi\bar{\chi}) \simeq 1$ and $m_a = 10$ keV. The shaded areas are ruled out from the existed experiments, and the solid lines correspond to the expected reaches of the fixed-target experiments. The red line is the projected sensitivity for NA64e experiment, the black line corresponds to the NA64μ facility, the blue line is the expected reach of M^3, and the green line corresponds to the projected sensitivity of the LDMX facility. The shaded red region shows the parameter space excluded by the NA64e experiment for EOT $\simeq 3 \times 10^{11}$. At a 90% C.L., the excluded region of the NA64e experiment rules out the possible explanation of $(g-2)$ muon (shaded orange region) and electron (shaded brown region) anomalies [3,97,98] by the minimal ALP scenario at the two-loop level [49]. The *BABAR* pink-shaded region refers to the search for the three-body monophoton process $e^+e^- \to a\gamma\gamma_D$ followed by the rapid decay into a DM pair $\gamma_D \to \chi\bar{\chi}$. The dark green line represents the expected reach of the NA64e experiment associated with J/ψ meson photoproduction followed by invisible decay $J/\psi \to a\gamma_D$ for EOT $\simeq 5 \times 10^{12}$.

Therefore, one can improve the sensitivity of the muon beam mode by increasing the typical interaction length of the dump.

C. Expected constraints from $J/\psi(1S) \to a\gamma_D$ decay at NA64e

In this subsection, we follow Ref. [66,101] to constrain the parameter space of the minimal ALP portal scenario from the invisible decay of $J/\psi \to a\gamma_D$ at NA64e. The matrix element of the charm quark and antiquark transition process $c(p_1)\bar{c}(p_2) \to \gamma^*(q) \to a(k_2)\gamma_D(k_1)$ can be written as follows (see, e.g., Fig. 7 for detail):

$$\mathcal{M}_{c\bar{c}} = ieQ_c\bar{v}(p_2)\gamma^\mu u(p_1)\frac{g_{\mu\nu}}{q^2}g_{a\gamma\gamma_D}\epsilon^{\nu\lambda\rho\sigma}k_{1\lambda}q_{2\rho}\epsilon_{\sigma(k_1)}, \quad (18)$$

where k_1, k_2 and p_1, p_2 are, respectively, the four momenta of the ALP, the dark photon, and of the charm quarks. In the center-of-mass frame, one has $p_1 = p_2 = p = (m_c, 0, 0, 0)$, with m_c being the mass of the charm quark, while q in Eq. (18) is the photon four-momentum, such that $q^2 = 4m_c^2$, $Q_c = 2/3$ is the charge of the charm quark. By integrating the averaged amplitude squared $\overline{|\mathcal{M}_{cc}|^2}$ [see, e.g., Eq. (18)] over the phase space of outgoing particles, one can obtain the invisible decay width

$$\Gamma_{J/\psi\to a\gamma_D} = \frac{|\psi_{J/\psi}(0)|^2}{8\pi}g_{a\gamma\gamma_D}^2 e^2 Q_c^2\left(1-\frac{m_{\gamma_D}^2}{M_{J/\psi}^2}\right)^3, \quad (19)$$

where $M_{J/\psi} \simeq 3.1$ GeV is the mass of J/ψ, and $|\psi_{J/\psi}(0)|^2 \simeq 4.47 \times 10^{-2}$ GeV^3 is the squared radial wave function [99] of J/ψ at the origin $r = 0$. In order to calculate $\overline{|\mathcal{M}_{cc}|^2}$, we exploit the state-of-the-art FeynCalc package [102] of Wolfram *Mathematica* [103]. In Eq. (19), we neglect the ALP mass, $m_{\gamma_D} \gg m_a$. The authors provide in Table II of Ref. [66] the number of expected J/ψ vector mesons, $N_{J/\psi} \simeq 1.1 \times 10^5$, produced for projected statistics EOT $\simeq 5 \times 10^{12}$ at NA64e. Therefore, one can easily estimate the expected reach on $\mathrm{Br}(J/\psi \to a\gamma_D) \lesssim 2.3/N_{J/\psi}$ at a 90% C.L. that implies no signal events of J/ψ invisible decays into an $a\gamma_D$ pair at NA64e for the background free case. Here we use the value for the total decay width $\Gamma_{J/\psi}^{\mathrm{tot}} \simeq 92.9$ keV from Ref. [99]. That yields the expected reach on the coupling $g_{a\gamma\gamma_D} \lesssim 5 \times 10^{-3}$ GeV^{-1} at the 90% C.L. for NA64e in the mass range of interest 1 MeV $\lesssim m_{\gamma_D} \lesssim 1$ GeV. In Fig. 11, we show the regarding expected limit that can rule out the limit of NA64e for $a\gamma_D$ pair production in the process $eZ \to eZ\gamma^*(\to a\gamma_D)$ for the same statistics, EOT $\simeq 5 \times 10^{12}$. Note that in the present analysis, we conservatively assume that the dominant channel of missing-energy events at NA64e is associated with the photoproduction of the J/ψ meson $\gamma Z \to ZJ/\psi$ followed by its rapid decay $J/\psi \to a\gamma_D$ in the detector of NA64e. The production of ρ, ω and ϕ vector mesons at NA64e is expected to be subdominant [66,104].

D. Bounds from monophoton *BABAR* data

The authors of Ref. [49] provide an explicit analysis of the monophoton signal for the process $e^+e^- \to a\gamma_D$ followed by the decay $\gamma_D \to a\gamma$ from *BABAR* data. They also provide the regarding exclusion limits (see, e.g., Fig. 4 from Ref. [49]) in the $(m_{\gamma_D}, g_{a\gamma\gamma_D})$ plane from the *BABAR* experiment. These limits are not relevant for our minimal benchmark scenario, since we suppose that γ_D decays rapidly into a $\chi\bar{\chi}$ pair with $\mathrm{Br}(\gamma_D \to \chi\bar{\chi}) \simeq 1$, and thus visible monophoton decays $\gamma_D \to a\gamma$ are suppressed, $\mathrm{Br}(\gamma_D \to a\gamma) \ll 1$. However, the three-body final-state process $e^+e^- \to a\gamma\gamma_D$

is kinematically allowed for our analysis. That reaction is subleading relative to the two-body final-state process $e^+e^- \to a\gamma_D$. The regarding suppression can be found in Fig. 3 of Ref. [49], which shows the total cross sections of the relevant processes as the function of mass m_{γ_D}. In particular, for the mass range 1 MeV $\lesssim m_{\gamma_D} \lesssim 1$ GeV and $g_{a\gamma\gamma_D} = 1\ \mathrm{GeV}^{-1}$, one has $\sigma_{\mathrm{tot}}(e^+e^- \to a\gamma_D) \simeq 1.2 \times 10^5$ pb and $\sigma_{\mathrm{tot}}(e^+e^- \to a\gamma\gamma_D) \simeq 6 \times 10^3$ pb for two-body and three-body final states, respectively. Therefore, it is straightforward to obtain the relevant-for-our-analysis limit on $g^{(3-\mathrm{body})}_{a\gamma\gamma_D}$ from the monophoton bound $g^{(2-\mathrm{body})}_{a\gamma\gamma_D} \simeq 2 \times 10^{-3}\ \mathrm{GeV}^{-1}$ shown in Fig. 4 of Ref. [49]. Namely, for the mass range of interest, 1 MeV $\lesssim m_{\gamma_D} \lesssim 1$ GeV, this yields

$$g^{(3-\mathrm{body})}_{a\gamma\gamma_D} \simeq g^{(2-\mathrm{body})}_{a\gamma\gamma_D} \times \left(\frac{\sigma_{\mathrm{tot}}(e^+e^- \to a\gamma_D)}{\sigma_{\mathrm{tot}}(e^+e^- \to a\gamma\gamma_D)}\right)^{1/2} \simeq 1.5 \times 10^{-2}\ \mathrm{GeV}^{-1}. \tag{20}$$

As expected [49,50], the experimental reach of *BABAR* weakens by a factor of approximately $\sqrt{20} \simeq 4.5$ for $\mathrm{Br}(\gamma_D \to \chi\bar{\chi}) \simeq 1$. In Fig. 11, we show the current constraint from the *BABAR* monophoton signal $e^+e^- \to a\gamma\gamma_D$ by the shaded pink region. It rules out the current experimental constraints of the NA64*e* experiment for EOT $\simeq 3 \times 10^{11}$.

VI. NONMINIMAL ALP HADROPHILIC SCENARIO

In this section, we calculate the cross-section dark photon production in the process $lZ \to lZ\gamma_D$ that is shown on the left side of Fig. 6 for the case of hadrophilic ALPs. That implies the benchmark coupling of the ALP and dark photons in the following form:

$$\mathcal{L} \supset \mathcal{L}_{\text{dark axion portal}} + \bar{\chi}(\gamma^\mu i\partial_\mu - g_D\gamma^\mu A'_\mu + m_\chi)\chi + \sum_{N=n,p} a\bar{N}(g^s_\psi + ig^p_\psi\gamma_5)N. \tag{21}$$

For the sake of simplicity, we consider benchmark universal scalar and pseudoscalar coupling of ALPs to nucleons, such that $g^s_p = g^s_n \equiv g^s$ and $g^p_p = g^p_n \equiv g^p$.

In order to calculate the cross section of dark photon–lepton production at nucleus (A, Z), where A is the nucleus mass number and Z is the charge of the nucleus, we use the equivalent photon approximation, which implies replacing the fast-moving leptons with photons following a distribution [105]

$$\gamma_l(x_\gamma, q^2_\perp) \simeq \frac{\alpha}{2\pi}\frac{1+(1-x_\gamma)^2}{x_\gamma}\frac{q^2_\perp}{(q^2_\perp + x^2_\gamma m^2_l)^2}, \tag{22}$$

where E_γ is the energy of the photon emitted by an incoming lepton; x is the fraction of the photon energy defined as $x_\gamma \equiv E_\gamma/E_l$, where E_l is the energy of the incoming lepton; m_l is the lepton mass; and $q_\perp$ is the photon transfer momentum. Note that $q^2_\perp$ is typically very small, $q_\perp \ll E_l, E_\gamma$. The total cross section of dark photon–lepton production at nucleus can be written as

$$\sigma_{lZ\to lZ\gamma_D} = \int dx\, dq^2_\perp \gamma_l(x_\gamma, q^2_\perp) \int dt \frac{d\sigma_{\gamma Z\to Z\gamma_D}}{dt}, \tag{23}$$

where the cross section of dark photon production can be written as the sum of partial cross sections for each nucleon N in the nucleus of the target:

$$\frac{d\sigma_{\gamma Z\to Z\gamma_D}}{dt} = A\frac{d\sigma_{\gamma N\to N\gamma_D}}{dt}.$$

The Lorentz-invariant form of the differential cross section of dark photon production due to photon scattering on the nucleon is

$$\frac{d\sigma_{\gamma N\to N\gamma_D}}{dt} = \frac{\frac{1}{4}\sum_{\mathrm{pol}}|M_{\gamma N}|^2}{16\pi\lambda(s, m^2_N, 0)}, \tag{24}$$

where $\lambda(s, m^2_N, 0) = (s - m^2_N)^2 = 4m^2_N E^2_\gamma$ is the Källen function in the rest frame of the initial nucleon. Then the square of the magnitude of the matrix element is given by

$$|M_{\gamma N}|^2 \simeq \frac{g^2_{a\gamma\gamma_D}}{2}\frac{(t - m^2_{\gamma_D})^2}{(t - m^2_a)^2}m^2_N \times \left[g^2_s - g^2_p + (g^2_s + g^2_p)\frac{E_{2N}}{m_N}\right], \tag{25}$$

where $E_{2N} \simeq m_N - t/(2m_N)$ is the energy of the outgoing nucleon in the laboratory frame and t is the nucleon transfer momentum squared, such that $t \equiv -2m_N(E_\gamma - E_{\gamma_D})$; for the nearly collinear emission of dark photons, this yields

$$t \simeq -E^2_\gamma\theta^2_{\gamma_D} - m^4_{\gamma_D}/(4E^2_\gamma).$$

It is worth mentioning that for the small angles of dark photon production, the amplitude squared Eq. (25) is suppressed if we set $g^s_N = 0$ and $g^p_N \neq 0$. The regarding suppression factor is associated with the term

$$|M_{\gamma N}|^2 \propto (g^p_N)^2(E_{2N} - m_N)/m_N \ll 1$$

as long as $\theta_{\gamma_D} \ll 1$ and $E_{2N} \simeq m_N$. Otherwise, if we set $g^p_N = 0$ and $g^s_N \neq 0$, one gets

$$|M_{\gamma N}|^2 \propto (g^s_N)^2 E_{2N}/m_N.$$

As a result, the cross section for the scalar-specific couplings of nucleons is enhanced by a factor of approximately $\simeq E_{2N}/(E_{2N} - m_N)$ relative to the pseudo-scalar-specific

cross section. If one sets $g_p = g_s = g_N$, then for $t \ll m_a^2, m_{\gamma_D}^2$, we get the following expression for the amplitude squared:

$$|M_{\gamma N}|^2 \simeq g_{a\gamma\gamma_D}^2 g_N^2 m_N^2 \left(\frac{m_{\gamma_D}}{m_a}\right)^4 \left[1 + \mathcal{O}\left(\frac{m_{\gamma_D}^2}{E_\gamma^2}\right)\right]. \quad (26)$$

Equation (26) implies that for the highly collinear emission of the dark photon (negligible momentum transfer), its production rate grows as $\propto (m_{\gamma_D}/m_a)^4$ for increasing m_{γ_D}. In fact, the nucleon momentum transfer cannot be completely neglected, and the realistic cross section grows a bit more slowly than $(m_{\gamma_D}/m_a)^4$ as $m_{\gamma_D} \gtrsim \mathcal{O}(100)$ MeV.

Finally, one can obtain the double differential cross section of dark photon production:

$$\frac{d\sigma_{lZ\to lZ\gamma_D}}{dE_{\gamma_D} d\theta_{\gamma_D}} \simeq \frac{1}{E_l} \int dq_\perp^2 \gamma_l(E_{\gamma_D}/E_l, q_\perp^2) \frac{d\sigma_{\gamma Z}}{d\theta_{\gamma_D}}. \quad (27)$$

In Fig. 12, we show the differential cross section $(d\sigma/d\theta_{\gamma_D})_{lZ\to lZ\gamma_D}$ as a function of θ_{γ_D} in the range of small dark photon emission angle $\theta_{\gamma_D} \lesssim 0.1$. As we mentioned above, the larger masses m_{γ_D} imply larger values of the differential cross section. That dependence can be described also in terms of specific Lorentz-invariant characteristics. Let us consider the characteristic function for the benchmark case [106]

$$g_{\gamma_D} = (s - m_N^2)/(s - m_{\gamma_D}^2 + m_N^2) \times \lambda^{\frac{1}{2}}(s, m_N^2, 0)/\lambda^{\frac{1}{2}}(s, m_{\gamma_D}^2, m_N^2), \quad (28)$$

which is associated with the typical angles of dark photon emission in the laboratory frame. It is straightforward to obtain that $g_{\gamma_D} > 1$ for $m_{\gamma_D} \lesssim 100$ MeV, which means that $\theta_{\gamma_D} \ll 1$—i.e., the cross section peaks forward. On the other hand, one can obtain that $g_{\gamma_D} < 1$ as soon as $m_{\gamma_D} \gtrsim 1$ GeV; therefore, the typical momentum of dark photon γ_D production cannot be collinear to the beam line in this case—i.e., the typical angles θ_{γ_D} can be as large as $\theta_{\gamma_D} \gtrsim 1$. In the present paper, we study the elastic production of dark photons, so that in the analysis for simplicity we conservatively set the typical maximum angle of dark photon emission to be $\theta_{\gamma_D} \lesssim \theta_{\max} \equiv 0.1$. The total cross section of the dark photon production is calculated for the regarding angle cut, which however decreases significantly the signal rate of γ_D emission.

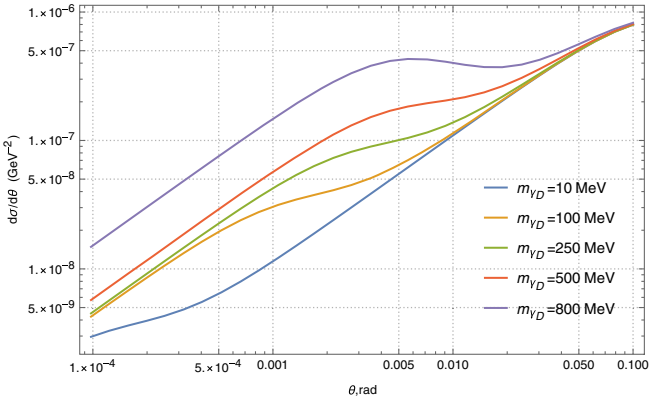

FIG. 12. The differential cross section by angle of dark photon production at a fixed target of NA64e in the hadrophilic ALP portal for various dark photon masses m_{γ_D} and for small values of angle θ between dark photons and photons from the beam. We set parameters as $m_a = 10$ keV, $g^s = g^p = 1$, $g_{a\gamma\gamma_D} = 1$ GeV^{-1}, $E_e = 100$ GeV.

However, for the ALP hadrophilic scenario, it is worth calculating the inelastic photoproduction cross section of γ_D that implies a large nucleon transfer momentum and a relatively wide emission angle $\theta_{\gamma_D} \gtrsim 1$. That analysis would require the realistic simulation of the experimental efficiency and the hadronic response in the detector. This, however, is beyond the scope of the present paper, and we leave such analysis for future study.

In Fig. 14 of Sec. VIII, the 90% C.L. sensitivity curves of the fixed-target experiments are shown for the combination of couplings $|g_{a\gamma\gamma_D} g_N|$. In order to plot these curves, we set $N_{\text{sign}} > 2.3$, implying Poisson statistics for the signal events, background free case, and null results for the DM detection.

VII. NONMINIMAL ALP LEPTOPHILIC SCENARIO

In this section, we consider the process

$$l(p)Z(\mathcal{P}_i) \to l(p')Z(\mathcal{P}_f)\gamma_D(k), \quad (29)$$

shown in the right panel of Fig. 6 for the leptophilic ALP, where $p = (E_l, \mathbf{p})$ and $p' = (E_l', \mathbf{p}')$ are the four-momenta of initial and outgoing leptons, respectively; $\mathcal{P}_i = (M_N, \mathbf{0})$ and $\mathcal{P}_f = (\mathcal{P}_f^0, \mathbf{P}_f)$ are the four-momenta of initial and outgoing nuclei, respectively; and here M_N is the mass of the nucleus and $k = (E_{\gamma_D}, \mathbf{k})$ is the four-momentum of a dark photon. The benchmark Lagrangian of that simplified ALP portal scenario can be written as follows:

$$\mathcal{L} \supset \mathcal{L}_{\text{dark axion portal}} + \bar{\chi}(\gamma^\mu i\partial_\mu - g_D\gamma^\mu A'_\mu + m_\chi)\chi + \sum_{l=e,\mu} i g_l^p a \bar{l}\gamma_5 l, \quad (30)$$

where we consider only the pseudoscalar coupling of the ALP to the leptons g_l^p. The numerical calculations reveal that the scalar coupling to leptons $\mathcal{L} \supset \sum_{l=e,\mu} g_l^s a\bar{l}l$ yields a similar contribution to the signal events if we set the universal coupling as $g_l^s = g_l^p$.

To calculate the cross section of the process in Eq. (29), we use the equivalent photon approximation [60,95,107], which implies a factorization of $2 \to 3$ rate into the product

of the photon flux and a $2 \to 2$ cross section of the Compton-like process $l(p)\gamma(q) \to l(p')\gamma_D(k)$:

$$\frac{d\sigma_{lZ\to lZ\gamma_D}}{d(pk)d(k\mathcal{P}_i)} \simeq \frac{\alpha\chi}{\pi(p'\mathcal{P}_i)} \cdot \frac{d\sigma_{l\gamma\to l\gamma_D}}{d(pk)}\bigg|_{t=t_{\min}}, \tag{31}$$

where χ is the effective photon flux from the nucleus [60]. In Eq. (31), we assume that the photon virtuality t has its minimum $t_{\min}$ when $\mathbf{q}$ is collinear with $\mathbf{k}-\mathbf{p}$. We define auxiliary Mandelstam variables, and regarding identity as follows:

$$\tilde{u} = (p-k)^2 - m_l^2, \qquad \tilde{s} = (p'+k)^2 - m_l^2, \tag{32}$$

$$t_2 = (p-p')^2, \qquad \tilde{s} + \tilde{u} + t_2 \simeq m_{\gamma_D}^2, \tag{33}$$

one can easily obtain the following expression for the differential cross section in the Lorentz-invariant notations [60,95,107]:

$$\frac{d\sigma_{2\to2}}{d(pk)} \simeq \frac{1}{8\pi\tilde{s}^2} \cdot \overline{|\mathcal{M}_{2\to2}|^2}. \tag{34}$$

Let us calculate now the amplitude of the relevant $2 \to 2$ subprocess

$$\mathcal{M}_{2\to2} = g_l^p g_{a\gamma\gamma_D} \frac{\bar{u}(p')\gamma_5 u(p)}{t_2 - m_a^2} \epsilon_\mu(q)\epsilon_\nu^*(k)\epsilon^{\mu\nu qk}, \tag{35}$$

where $\epsilon^{\mu\nu qk} = q_\lambda k_\rho \epsilon^{\mu\nu\lambda\rho}$. As the result of averaging over polarizations, one gets the following expression for the amplitude squared:

$$\begin{aligned}\overline{|\mathcal{M}_{2\to2}|^2} &= \frac{1}{4}\sum_{\text{pol}} |\mathcal{M}_{2\to2}|^2 \\ &= -\frac{1}{4}\frac{(g_l^p)^2 g_{a\gamma\gamma_D}^2}{(t_2 - m_a^2)^2} t_2 \lambda(t_2, 0, m_{\gamma_D}^2),\end{aligned} \tag{36}$$

where $\lambda(x,y,z) = x^2 + y^2 + z^2 - 2xy - 2xz - 2yz$ is the kinematical triangle Källen function. These calculations are performed by exploiting the state-of-the-art FeynCalc package [102] of Wolfram *Mathematica* [103].

It is worth noting that longitudinal term $k_\mu k_\mu / m_{\gamma_D}^2$ in the dark photon polarization tensor $\sum_i \epsilon_\mu^{*i}(k)\epsilon_\nu^i(k)$ does not contribute to the matrix element squared due to the current conservation. We label the energy fraction of the γ_D boson by $x = E_{\gamma_D}/E_l$ and the angle between $\mathbf{k}$ and $\mathbf{p}$ by θ_{γ_D}. Let us introduce the auxiliary function U as follows:

$$U \equiv -\tilde{u} \simeq E_l^2\theta_{\gamma_D}^2 x + m_{\gamma_D}^2(1-x)/x + m_l^2 x. \tag{37}$$

In Eq. (37), we keep only leading terms in $m_{\gamma_D}^2/E_{\gamma_D}^2$, m_l^2/E_l^2, $m_l^2/E_l'^2$, and $\theta_{\gamma_D}^2$. In the latter approach, one has

$$t_{\min} \simeq U^2/(4E_l^2(1-x)^2), \tag{38}$$

$$\tilde{s} \simeq U/(1-x), \qquad t_2 \simeq -xU/(1-x) + m_{\gamma_D}^2. \tag{39}$$

Finally, we obtain the expression for the double differential cross section:

$$\frac{d\sigma_{2\to3}}{dx d\cos\theta_{\gamma_D}} \simeq \frac{\alpha\chi}{\pi(1-x)} \cdot E_l^2 x \beta_{\gamma_D} \cdot \frac{d\sigma_{2\to2}}{d(pk)}, \tag{40}$$

where $\beta_{\gamma_D} = (1 - m_{\gamma_D}^2/(xE_l)^2)^{1/2}$ is the velocity of the dark photon in the laboratory frame. The explicit analytical expression for the effective photon flux χ is given in Ref. [60] for the case of an elastic form factor $G_{el}(t)$ that is proportional to $\propto Z^2$. An inelastic form factor $G_{\text{inel}}(t) \propto Z$, and for the heavy target nuclei $Z \propto \mathcal{O}(100)$, so one can safely ignore it in the calculation below.

The resulting cross section can be rewritten as

$$\begin{aligned}\frac{d\sigma_{2\to3}}{dx d\cos\theta_{\gamma_D}} \simeq \frac{\alpha\chi}{32\pi^2} E_l^2 \beta_{\gamma_D} (g_l^p)^2 g_{a\gamma\gamma_D}^2 \\ \times \frac{x^3[xU - m_{\gamma_D}^2(1-x)]}{[xU - (1-x)(m_{\gamma_D}^2 - m_a^2)]^2}.\end{aligned} \tag{41}$$

As an example, in Fig. (13) we show the differential cross sections of the process $eZ \to eZ\gamma_D$ as a function of x for the NA64e experiment and the benchmark ALP leptophilic setup [Eq. (30)] with $m_a = 10$ keV. The WW approximation for the leptophilic cross section implies that the photon flux χ from the nucleus is the function of x and θ_{γ_D}, so it is a fairly accurate approach for the exact tree-level cross section (for details, see, e.g., Ref. [60] and references therein).

In Fig. 15 in Sec. VIII, the 90% C.L. sensitivity curves of the fixed-target experiments are shown for the combination of couplings $|g_{a\gamma\gamma_D} g_l^p|$. To plot these curves, we set

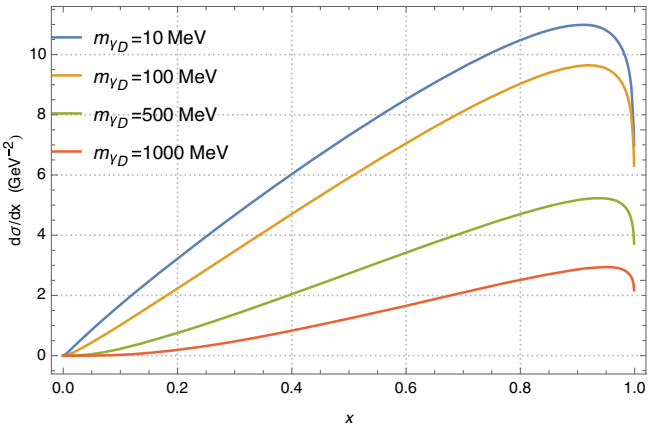

FIG. 13. The differential cross section of dark photon production at NA64e as a function of the fraction energy $x = E_{\gamma_D}/E_l$ for the ALP leptophilic scenario and for various masses m_{γ_D}. We set $m_a = 10$ keV, $g_l^p = 1$, $g_{a\gamma\gamma_D} = 1$ GeV^{-1}, and $E_e = 100$ GeV.

$N_{\rm sign} > 2.3$, implying a null result for the DM detection and background free case.

VIII. SUMMARY AND DISCUSSION

In the present paper, in addition to the ALP contribution to lepton EDMs, we have calculated the novel limits on the combination of CP-even and CP-odd couplings of neutrons with ALPs from the current constraints on neutron EDMs by taking into account their anomalous magnetic moments. The regarding contribution to neutron EDM is associated with a light scalar/pseudoscalar boson exchange at the one-loop level. This contribution is proportional to $\sim\bar{\theta}$ of the QCD parameter of CP violation [80,81]. In addition, we have considered the possible implication of dark axion portal couplings to the EDM of SM fermions. In particular, we have calculated at the one-loop level the EDM that can be induced by the three specific model-independent interactions: (i) CP-odd Yukawa-like couplings of ALP with fermions, (ii) CP-even interaction of SM fermions and light vector bosons, and (iii) CP-even dark axion/ALP portal couplings. Such Barr-Zee-type diagrams have ultraviolet (UV) logarithmic divergences, which can be calculated by using the $\overline{\rm MS}$ regularization scheme and removed by exploiting the local counterterms of the EDM type. We briefly discuss the regarding renormalization procedure in Appendix B.

We have also discussed in detail the probing of the dark ALP portal scenario through the dark photon decaying predominantly to the DM particles, $\mathrm{Br}(\gamma_D \to \chi\bar{\chi}) \simeq 1$. In the present paper, we refer to the relevant benchmark model as the minimal dark ALP portal scenario (see bounds for $g_{a\gamma\gamma_D}$ coupling in Fig. 11). This scenario implies that the dark photon is a $U_D(1)$ gauge field and serves as the mediator between DM and SM particles through the dark axion portal. In this scenario, we imply that $m_a \ll m_{\gamma_D}$; therefore, the visible decay $a \to \gamma\gamma_D$ is kinematically forbidden.

We have studied in detail the missing-energy signatures for the projected and existing lepton fixed-target facilities, such as NA64e, LDMX, NA64μ, and M^3. In particular, by using the state-of-the-art CalcHEP package, we calculated the $a\gamma_D$ pair production cross sections in the processes $lZ \to lZa\gamma_D$ followed by the invisible dark photon decay into DM particles $\gamma_D \to \chi\bar{\chi}$ for the specific fixed-target facility. We have calculated the sensitivity curves for these experiments using the null result for DM detection for the existing and planned statistics of leptons accumulated on the target, the so-called invisible mode.

We have discussed in detail the expected reach of the NA64e experiment to probe the dark photon emission via the missing-energy process of vector meson production $eZ \to eZJ/\psi$ followed by invisible decay $J/\psi \to a\gamma_D(\to \chi\bar{\chi})$. We have shown that the latter signal process dominates over the bremsstrahlung $a\gamma_D$ pair emission in the reaction $eZ \to eZ\gamma^*(\to a\gamma_D)$ at NA64e. Thus, the expected reach of NA64e from $J/\psi \to a\gamma_D$ can rule out the projected bounds from the off-shell photon emission for EOT $\simeq 5 \times 10^{12}$.

We have recast the *BABAR* monophoton data $e^+e^- \to a\gamma\gamma_D$ to derive constraints on the dark ALP portal coupling, implying that the dark photon decays mainly to the DM fermion pair. We have shown that the existing

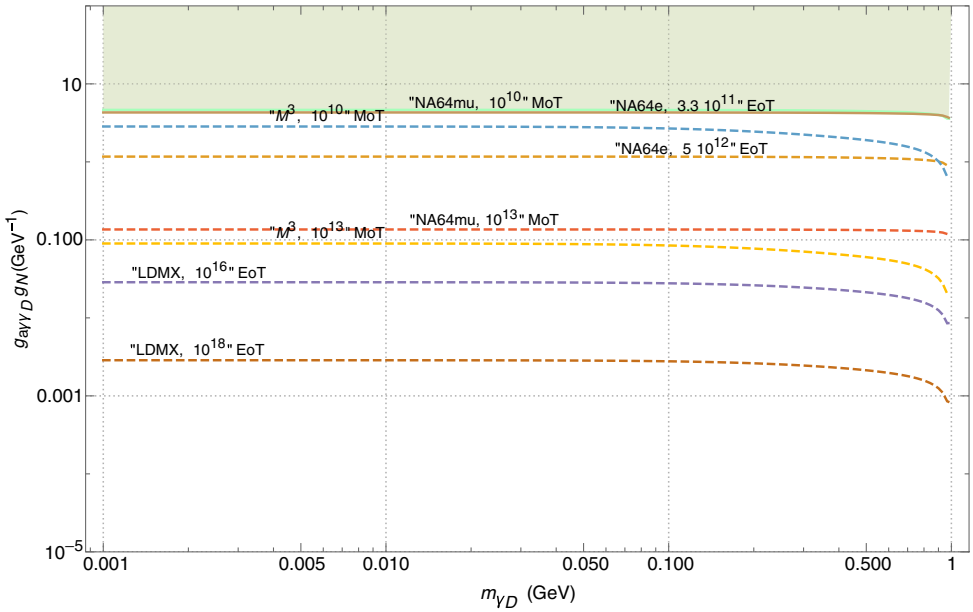

FIG. 14. Bounds on the combination of ALP couplings with gauge fields $g_{a\gamma\gamma_D}$ and ALP couplings with nucleons $g^s = g^p = g_N$ for the hadrophilic channel from current and proposal statistics of the experiments NA64e, NA64μ, LDMX, and M^3. We set here $\mathrm{Br}(\gamma_D \to \chi\bar{\chi}) \simeq 1$ and $m_a = 10$ keV.

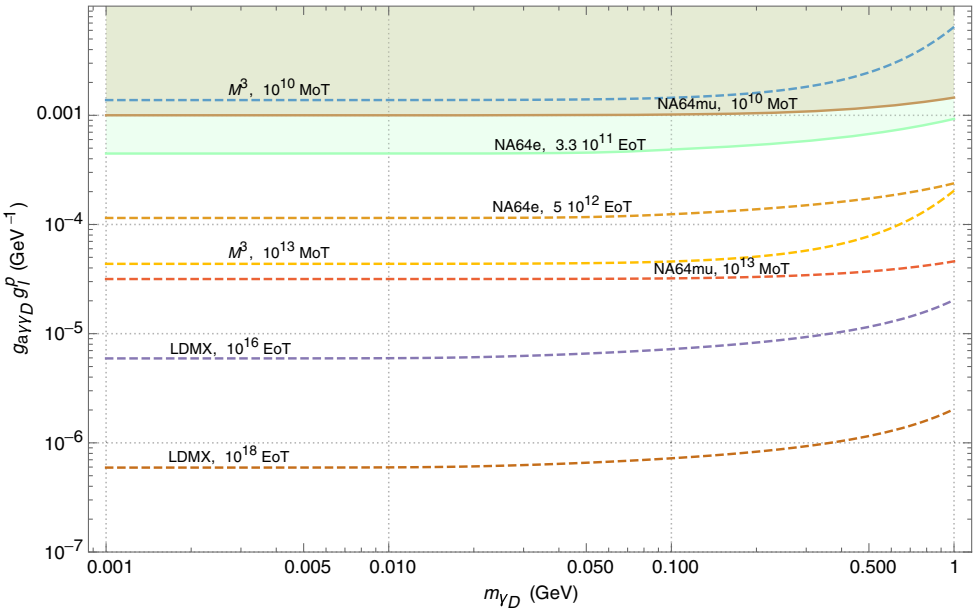

FIG. 15. Bounds on the combination of ALP couplings with leptons g_l^p and with gauge fields $g_{a\gamma\gamma_D}$ for the leptophilic scenario from current and proposal statistics of the NA64e, NA64μ, LDMX, and M^3 experiments. We set here $m_a = 10$ keV and $\mathrm{Br}(\gamma_D \to \chi\bar{\chi}) \simeq 1$.

BABAR bounds rule out the current NA64e constraints for EOT $\simeq 3 \times 10^{11}$.

We have considered the modifications of the minimal dark ALP portal scenario by including two benchmark Lagrangians in the model: hadron- and lepton-specific couplings which imply ALP Yukawa-like interaction mainly with hadrons and leptons, respectively. For both hadron- and lepton-specific scenarios we have calculated the cross sections of dark photon production $lZ \to lZ\gamma_D$ by using WW approximation. Calculation in WW approximation is in a reasonable agreement with the exact tree-level calculation performed with CalcHEP. We note that for the specific parameter space, there are missing-energy channels that originate also from meson decay $(J/ \to a\gamma_D)$ and bremsstrahlung $(\gamma^* \to a\gamma_D)$ in both hadrophilic and leptophilic scenarios. However, in order to distinguish them from the minimal scenario, we set the conservative upper bounds on the specific (hadron and leptonic) combination of couplings by considering the channel $lZ \to lZ\gamma_D$ as the dominant one. We plan to calculate the contribution of $J/ \to a\gamma_D$ and $\gamma^* \to a\gamma_D$ for the fermion-specific ALPs in the forthcoming paper [86].

The calculations reveal the differences between hadrophilc and leptophilic cross sections of dark photon production. First, the ALP hadrophilic cross section is relatively small, since it scales to the first power of the nucleon/atomic number $\propto A$. Contrarily, the ALP leptophilic rate of γ_D production is enhanced due to the factor $\propto Z^2$. Second, the hadrophilic cross section is sensitive to the cut on the angle of dark photon emission θ_{γ_D}. A large θ_{γ_D} leads to the inelastic scattering that is associated with significant transfer momentum to nucleons. Because of this, in the present analysis we conservatively set the upper benchmark value $\theta_{\gamma_D} \lesssim \theta_{\gamma_D}^{\max} \simeq 0.1$ rad in order to get rid of the inelastic interaction of ALP with nucleus matter. On the other hand, the leptophilic cross section $d\sigma_{2\to3}/dx$ depends weakly on $\theta_{\gamma_D}^{\max}$, since $d\sigma_{2\to3}/d\theta_{\gamma_D}$ has a very narrow peak at the typical angles of dark photon emission $\theta_{\gamma_D} \simeq m_l/E_l \ll 1$.

Moreover, we want to note that the total cross section for the hadrophilic scenario is suppressed relative to the leptophilic one. The suppression factor is estimated to be of the order of $\sim 10^{-7} \div 10^{-5}$. Thus, the resulting hadrophilc constraints are weaker than leptophilic bounds for the same number of leptons accumulated on target. That difference can be found in both Figs. 14 and 15, where the bounds on the combination of couplings for the hadrophilic and leptophilic scenarios are depicted, respectively. In the framework of considered benchmark scenarios, the most stringent constraints on the couplings are expected from the projected experiment LDMX.

In the future, we plan to consider also the possible benchmark dark ALP portal signatures along with both ALP portal and vector portal scenarios.

ACKNOWLEDGMENTS

We would like to thank N. Arefyeva, R. Capdevilla, A. Celentano, X. Chu, P. Crivelli, S. Demidov, D. Forbes, S. Gninenko, D. Gorbunov, Y. Kahn, M. Kirsanov, N. Krasnikov, G. Krnjaic, L. Molina Bueno, A. Pimikov, J. Pradler, A. Pukhov, P. Schuster, H. Sieber, and F. Tkachov for very helpful discussions and correspondences. This work was funded by BMBF (Germany) "Verbundark photon projekt 05P2021 (ErUM-FSP T01)—Run 3 von

ALICE am LHC: Perturbative Berechnungen von Wirkungsquerschnitten für ALICE" (Förderkennzeichen: 05P21VTCAA), by ANID PIA/APOYO AFB180002 (Chile), by FONDECYT (Chile) under Grant No. 1191103, and by ANID—Millennium Program—ICN2019_044 (Chile). This research was supported by TSU and TPU development programs. The work of A. S. Z. is supported by AYSS JINR (Grant No. 22-302-02). The work of D. V. K. on the description of the dark matter missing-energy signatures of NA64*e* and regarding exclusion limits for the minimal dark axion portal scenario is supported by Russian Science Foundation RSF Grant No. 21-12-00379.

APPENDIX A: ANALYTIC FORM OF LOOP INTEGRAL

Here we present the analytic form for loop integrals [Eqs. (6) and (8)] which are used for fermion EDM calculation:

$$g_1(y) = 1 - y^2 \log y - \frac{y(y^2-2)}{2\sqrt{y^2-4}}\left(\arctan\left(\frac{y^2-2}{y\sqrt{y^2-4}}\right) - \arctan\left(\frac{y}{\sqrt{y^2-4}}\right)\right), \tag{A1}$$

$$g_2(y) = k_n\left\{\frac{3}{2} - y^2 + (y^2-3)y^2\log y + \frac{\sqrt{y^2-4}}{2}(y^2-2)y\left(\arctan\frac{y}{\sqrt{y^2-4}} + \arctan\frac{2-y^2}{y\sqrt{y^2-4}}\right)\right.$$
$$\left. + \frac{y^3}{2}\sqrt{y^2-4}\left(\arctan\frac{y}{\sqrt{y^2-4}} - \arctan\frac{2-y^2}{y\sqrt{y^2-4}}\right)\right\}. \tag{A2}$$

APPENDIX B: LEPTON EDM INDUCED BY THE BARR-ZEE DIAGRAMS WITH THE LEPTON–DARK PHOTON–AXION LOOP

Here we consider details of the calculation of the correction to the lepton EDM induced by Barr-Zee diagrams with the lepton–dark photon–axion loop. In order to remove the logarithmic divergence contained in the Barr-Zee diagrams, we add the local counterterm, which is induced by the following Lagrangian:

$$\mathcal{L}_{\rm ct} = g_{\rm ct}(\mu) F_{\mu\nu}\bar{l} i\sigma^{\mu\nu}\gamma^5 l, \tag{B1}$$

where $g_{\rm ct}(\mu)$ is the coupling constant depending on the renormalization scale μ. In particular, we choose $g_{\rm ct}(\mu)$ as

$$g_{\rm ct}(\mu) = g\left[\frac{1}{\bar{\epsilon}} - \gamma\log\frac{m_l^2}{\mu^2}\right], \tag{B2}$$

where m_l is the lepton mass, and g and γ are the parameters, which will be fixed to drop divergence in the Barr-Zee diagrams and guarantee scale independence of the result for lepton EDM. Here, $\bar{\epsilon}$ is the pole in the $\overline{\rm MS}$ renormalization scheme:

$$\frac{1}{\bar{\epsilon}} = \frac{1}{\epsilon} + \Gamma'(1) - \log(4\pi). \tag{B3}$$

Therefore, the contribution of the counterterm to the lepton EDM is

$$d_l^{\rm ct} = -2g\left[\frac{1}{\bar{\epsilon}} + \gamma\log\frac{m_l^2}{\mu^2}\right]. \tag{B4}$$

The contribution of the Barr-Zee diagrams to the lepton EDM reads

$$d_l^{BZ} = \frac{G}{8\pi^2}\left[\frac{1}{\bar{\epsilon}} - \int_0^1 d^3\alpha \log\frac{\Delta}{\mu^2}\right], \tag{B5}$$

where $G = g_{a\gamma\gamma_D} g_s e\epsilon$ is the effective coupling, which is the product of three respective couplings between photons, dark photons, axions, and leptons [see, e.g., Eq. (10) for details]:

$$\Delta = m_{A'}^2\alpha_1 + m_a^2\alpha_2 + m_l^2\alpha_3^2, \tag{B6}$$

where

$$\int_0^1 d^3\alpha \equiv \int_0^1 d\alpha_1 \int_0^1 d\alpha_2 \int_0^1 d\alpha_3 \delta\left(1 - \sum_{i=1}^3 \alpha_i\right). \tag{B7}$$

The result for the lepton EDM can be written as

$$d_l = d_l^{\rm BZ} + d_l^{\rm ct} = \frac{2}{\bar{\epsilon}}\left[\frac{G}{16\pi^2} - g\right]$$
$$- 2\log\frac{m_l^2}{\mu^2}\left[\frac{G}{16\pi^2} - g\gamma\right] - \frac{G}{4\pi^2}\int_0^1 d^3\alpha \log\frac{\Delta}{\mu^2}. \tag{B8}$$

From Eq. (B8), it follows that the couplings g and γ must be fixed as

$$g = \frac{G}{16\pi^2}, \qquad \gamma = 1. \tag{B9}$$

Finally, one gets

$$d_l = -\frac{G}{4\pi^2}\int_0^1 d^3\alpha \, \log\frac{\Delta}{\mu^2}. \tag{B10}$$

After integration over two Feynman parameters, we have

$$d_l = -\frac{G}{4\pi^2}\left[-\frac{1}{2} + \frac{I(m_{A'}^2) - I(m_a^2)}{m_{A'}^2 - m_a^2}\right], \tag{B11}$$

where

$$I(m^2) = \int_0^1 dx[m^2(1-x) + m_l^2 x^2] \times \log\frac{m^2(1-x) + m_l^2 x^2}{\mu^2}. \tag{B12}$$

Next, it is interesting to consider a few limiting cases:

(1) $m_l = 0$:

$$d_l = -\frac{G}{4\pi^2}\left[-1 + \frac{I_0(m_{A'}^2) - I_0(m_a^2)}{m_{A'}^2 - m_a^2}\right], \tag{B13}$$

where

$$I_0(m^2) = m^2(1-x)\log\frac{m^2}{\mu^2}. \tag{B14}$$

(2) $m_l = 0$, $m_{A'} = m_a = m$:

$$d_l = -\frac{G}{8\pi^2}\left[-1 + \log\frac{m^2}{\mu^2}\right]. \tag{B15}$$

[1] R. D. Peccei and H. R. Quinn, Phys. Rev. D **16**, 1791 (1977).
[2] L. Di Luzio, M. Giannotti, E. Nardi, and L. Visinelli, Phys. Rep. **870**, 1 (2020).
[3] T. Aoyama *et al.*, Phys. Rep. **887**, 1 (2020).
[4] A. E. Dorokhov, A. E. Radzhabov, and A. S. Zhevlakov, JETP Lett. **100**, 133 (2014).
[5] C. Boehm and P. Fayet, Nucl. Phys. **B683**, 219 (2004).
[6] M. J. Dolan, F. Kahlhoefer, C. McCabe, and K. Schmidt-Hoberg, J. High Energy Phys. 03 (2015) 171; 07 (2015) 103(E).
[7] Y. Hochberg, E. Kuflik, R. Mcgehee, H. Murayama, and K. Schutz, Phys. Rev. D **98**, 115031 (2018).
[8] C. Han, M. L. López-Ibáñez, A. Melis, O. Vives, and J. M. Yang, Phys. Rev. D **103**, 035028 (2021).
[9] H. Davoudiasl, R. Marcarelli, and E. T. Neil, arXiv: 2112.04513.
[10] S. N. Gninenko and N. V. Krasnikov, Phys. Rev. D **106**, 015003 (2022).
[11] M. Bauer, M. Neubert, S. Renner, M. Schnubel, and A. Thamm, J. High Energy Phys. 04 (2021) 063.
[12] K. Choi, S. H. Im, and C. Sub Shin, Annu. Rev. Nucl. Part. Sci. **71**, 225 (2021).
[13] R. R. Dusaev, D. V. Kirpichnikov, and M. M. Kirsanov, Phys. Rev. D **102**, 055018 (2020).
[14] D. Banerjee *et al.* (NA64 Collaboration), Phys. Rev. Lett. **125**, 081801 (2020).
[15] H. Ishida, S. Matsuzaki, and Y. Shigekami, Phys. Rev. D **103**, 095022 (2021).
[16] Y. Sakaki and D. Ueda, Phys. Rev. D **103**, 035024 (2021).
[17] V. Brdar, B. Dutta, W. Jang, D. Kim, I. M. Shoemaker, Z. Tabrizi, A. Thompson, and J. Yu, Phys. Rev. Lett. **126**, 201801 (2021).
[18] D. Salnikov, P. Satunin, D. V. Kirpichnikov, and M. Fitkevich, J. High Energy Phys. 03 (2021) 143.
[19] Z. Bogorad, A. Hook, Y. Kahn, and Y. Soreq, Phys. Rev. Lett. **123**, 021801 (2019).
[20] Y. Kahn, B. Giaccone, A. Lunin, A. Netepenko, R. Pilipenko, and M. Wentzel, Proc. SPIE Int. Soc. Opt. Eng. **12016**, 29 (2022).
[21] L. Darmé, F. Giacchino, E. Nardi, and M. Raggi, J. High Energy Phys. 06 (2021) 009.
[22] P. S. B. Dev, D. Kim, K. Sinha, and Y. Zhang, Phys. Rev. D **104**, 035037 (2021).
[23] H. Abramowicz *et al.*, Eur. Phys. J. Special Topics **230**, 2445 (2021).
[24] J.-F. Fortin, H.-K. Guo, S. P. Harris, D. Kim, K. Sinha, and C. Sun, Int. J. Mod. Phys. D **30**, 2130002 (2021).
[25] K. Asai, S. Iwamoto, Y. Sakaki, and D. Ueda, J. High Energy Phys. 09 (2021) 183.
[26] R. Balkin, M. W. Krasny, T. Ma, B. R. Safdi, and Y. Soreq, Ann. Phys. (Berlin) **534**, 2100222 (2022).
[27] N. Blinov, E. Kowalczyk, and M. Wynne, J. High Energy Phys. 02 (2022) 036.
[28] I. Larin *et al.* (PrimEx Collaboration), Phys. Rev. Lett. **106**, 162303 (2011).
[29] S. N. Gninenko, N. V. Krasnikov, M. M. Kirsanov, and D. V. Kirpichnikov, Phys. Rev. D **94**, 095025 (2016).
[30] D. Banerjee *et al.* (NA64 Collaboration), Phys. Rev. Lett. **118**, 011802 (2017).

[31] S. N. Gninenko, D. V. Kirpichnikov, M. M. Kirsanov, and N. V. Krasnikov, Phys. Lett. B **782**, 406 (2018).
[32] S. N. Gninenko, D. V. Kirpichnikov, M. M. Kirsanov, and N. V. Krasnikov, Phys. Lett. B **796**, 117 (2019).
[33] D. Banerjee *et al.*, Phys. Rev. Lett. **123**, 121801 (2019).
[34] Y. M. Andreev *et al.*, Phys. Rev. D **104**, L091701 (2021).
[35] Y. M. Andreev *et al.* (NA64 Collaboration), Phys. Rev. Lett. **126**, 211802 (2021).
[36] I. Galon, E. Kajamovitz, D. Shih, Y. Soreq, and S. Tarem, Phys. Rev. D **101**, 011701 (2020).
[37] N. Blinov, G. Krnjaic, and D. Tuckler, Phys. Rev. D **103**, 035030 (2021).
[38] T. D. Beattie *et al.*, Nucl. Instrum. Methods Phys. Res., Sect. A **896**, 24 (2018).
[39] R. Essig *et al.*, in Community Summer Study 2013: Snowmass on the Mississippi, 2013, arXiv:1311.0029.
[40] G. Arcadi, A. Djouadi, and M. Raidal, Phys. Rep. **842**, 1 (2020).
[41] F. Fortuna, P. Roig, and J. Wudka, J. High Energy Phys. 02 (2021) 223.
[42] A. J. Buras, A. Crivellin, F. Kirk, C. A. Manzari, and M. Montull, J. High Energy Phys. 06 (2021) 068.
[43] A. Kachanovich, S. Kovalenko, S. Kuleshov, V. E. Lyubovitskij, and A. S. Zhevlakov, Phys. Rev. D **105**, 075004 (2022).
[44] M. Escudero, N. Rius, and V. Sanz, J. High Energy Phys. 02 (2017) 045.
[45] Y. Nomura and J. Thaler, Phys. Rev. D **79**, 075008 (2009).
[46] K. Kaneta, H.-S. Lee, and S. Yun, Phys. Rev. Lett. **118**, 101802 (2017).
[47] K. Kaneta, H.-S. Lee, and S. Yun, Phys. Rev. D **95**, 115032 (2017).
[48] J. C. Gutiérrez, B. J. Kavanagh, N. Castelló-Mor, F. J. Casas, J. M. Diego, E. Martínez-González, and R. V. Cortabitarte, arXiv:2112.11387.
[49] P. deNiverville, H.-S. Lee, and M.-S. Seo, Phys. Rev. D **98**, 115011 (2018).
[50] P. deNiverville and H.-S. Lee, Phys. Rev. D **100**, 055017 (2019).
[51] S. Alekhin *et al.*, Rep. Prog. Phys. **79**, 124201 (2016).
[52] J. L. Feng *et al.*, arXiv:2203.05090.
[53] P. Deniverville, H.-S. Lee, and Y.-M. Lee, Phys. Rev. D **103**, 075006 (2021).
[54] V. Domcke, K. Schmitz, and T. You, arXiv:2108.11295.
[55] S.-F. Ge, X.-D. Ma, and P. Pasquini, Eur. Phys. J. C **81**, 787 (2021).
[56] D. V. Kirpichnikov, V. E. Lyubovitskij, and A. S. Zhevlakov, Phys. Rev. D **102**, 095024 (2020).
[57] D. V. Kirpichnikov, V. E. Lyubovitskij, and A. S. Zhevlakov, Particles **3**, 719 (2020).
[58] S. N. Gninenko, N. V. Krasnikov, and V. A. Matveev, Phys. Rev. D **91**, 095015 (2015).
[59] S. N. Gninenko and N. V. Krasnikov, Phys. Lett. B **783**, 24 (2018).
[60] D. V. Kirpichnikov, H. Sieber, L. M. Bueno, P. Crivelli, and M. M. Kirsanov, Phys. Rev. D **104**, 076012 (2021).
[61] H. Sieber, D. Banerjee, P. Crivelli, E. Depero, S. N. Gninenko, D. V. Kirpichnikov, M. M. Kirsanov, V. Poliakov, and L. Molina Bueno, Phys. Rev. D **105**, 052006 (2022).
[62] J. Mans (LDMX Collaboration), EPJ Web Conf. **142**, 01020 (2017).
[63] A. Berlin, N. Blinov, G. Krnjaic, P. Schuster, and N. Toro, Phys. Rev. D **99**, 075001 (2019).
[64] T. Åkesson *et al.* (LDMX Collaboration), arXiv:1808.05219.
[65] A. M. Ankowski, A. Friedland, S. W. Li, O. Moreno, P. Schuster, N. Toro, and N. Tran, Phys. Rev. D **101**, 053004 (2020).
[66] P. Schuster, N. Toro, and K. Zhou, Phys. Rev. D **105**, 035036 (2022).
[67] T. Åkesson *et al.*, in 2022 Snowmass Summer Study, 2022, arXiv:2203.08192.
[68] Y. Kahn, G. Krnjaic, N. Tran, and A. Whitbeck, J. High Energy Phys. 09 (2018) 153.
[69] R. Capdevilla, D. Curtin, Y. Kahn, and G. Krnjaic, J. High Energy Phys. 04 (2022) 129.
[70] B. Holdom, Phys. Lett. **166B**, 196 (1986).
[71] J. F. Gunion, H. E. Haber, G. L. Kane, and S. Dawson, Front. Phys. **80**, 1 (2000).
[72] A. Djouadi, Phys. Rep. **459**, 1 (2008).
[73] G. C. Branco, P. M. Ferreira, L. Lavoura, M. N. Rebelo, M. Sher, and J. P. Silva, Phys. Rep. **516**, 1 (2012).
[74] E. J. Chun and T. Mondal, J. High Energy Phys. 07 (2021) 044.
[75] V. A. Dzuba, V. V. Flambaum, I. B. Samsonov, and Y. V. Stadnik, Phys. Rev. D **98**, 035048 (2018).
[76] V. Flambaum, S. Lambert, and M. Pospelov, Phys. Rev. D **80**, 105021 (2009).
[77] H. Yan, G. A. Sun, S. M. Peng, H. Guo, B. Q. Liu, M. Peng, and H. Zheng, Eur. Phys. J. C **79**, 971 (2019).
[78] C. A. J. O'Hare and E. Vitagliano, Phys. Rev. D **102**, 115026 (2020).
[79] P. A. Zyla *et al.* (Particle Data Group), Prog. Theor. Exp. Phys. **2020**, 083C01 (2020).
[80] A. S. Zhevlakov and V. E. Lyubovitskij, Phys. Rev. D **101**, 115041 (2020).
[81] R. J. Crewther, P. Di Vecchia, G. Veneziano, and E. Witten, Phys. Lett. **88B**, 123 (1979); **91B**, 487(E) (1980).
[82] A. S. Zhevlakov, M. Gorchtein, A. N. Hiller Blin, T. Gutsche, and V. E. Lyubovitskij, Phys. Rev. D **99**, 031703 (2019).
[83] A. S. Zhevlakov, T. Gutsche, and V. E. Lyubovitskij, Phys. Rev. D **99**, 115004 (2019).
[84] T. Gutsche, A. N. Hiller Blin, S. Kovalenko, S. Kuleshov, V. E. Lyubovitskij, M. J. Vicente Vacas, and A. Zhevlakov, Phys. Rev. D **95**, 036022 (2017).
[85] D. E. Maison and L. V. Skripnikov, Phys. Rev. A **105**, 032813 (2022).
[86] D. V. Kirpichnikov, V. E. Lyubovitskij, and A. S. Zhevlakov (to be published).
[87] A. Belyaev, N. D. Christensen, and A. Pukhov, Comput. Phys. Commun. **184**, 1729 (2013).
[88] V. M. Budnev, I. F. Ginzburg, G. V. Meledin, and V. G. Serbo, Phys. Rep. **15**, 181 (1975).
[89] R. Engel, A. Schiller, and V. G. Serbo, Z. Phys. C **71**, 651 (1996).
[90] M. I. Vysotsky and E. Zhemchugov, Phys. Usp. **62**, 910 (2019).
[91] M. Bondi, A. Celentano, R. R. Dusaev, D. V. Kirpichnikov, M. M. Kirsanov, N. V. Krasnikov, L. Marsicano, and D. Shchukin, Comput. Phys. Commun. **269**, 108129 (2021).

[92] X. Chu, J. Pradler, and L. Semmelrock, Phys. Rev. D **99**, 015040 (2019).
[93] C.-Y. Chen, M. Pospelov, and Y.-M. Zhong, Phys. Rev. D **95**, 115005 (2017).
[94] S. N. Gninenko, D. V. Kirpichnikov, and N. V. Krasnikov, Phys. Rev. D **100**, 035003 (2019).
[95] J. D. Bjorken, R. Essig, P. Schuster, and N. Toro, Phys. Rev. D **80**, 075018 (2009).
[96] Y.-S. Tsai, Phys. Rev. D **34**, 1326 (1986).
[97] B. Abi *et al.* (Muon $g-2$ Collaboration), Phys. Rev. Lett. **126**, 141801 (2021).
[98] R. H. Parker, C. Yu, W. Zhong, B. Estey, and H. Müller, Science **360**, 191 (2018).
[99] P. A. Zyla *et al.* (Particle Data Group), Prog. Theor. Exp. Phys. **2020**, 083C01 (2020).
[100] I. R. Blokland, A. Czarnecki, and K. Melnikov, Phys. Rev. Lett. **88**, 071803 (2002).
[101] A. Mangoni, Hadronic decays of the J/psi meson, Ph.D. thesis, Universita' Di Perugia, 2020, arXiv:2002.09675.
[102] V. Shtabovenko, R. Mertig, and F. Orellana, Comput. Phys. Commun. **207**, 432 (2016).
[103] W. R. Inc., Mathematica, Version 13.0.0, Champaign, IL, 2021.
[104] N. Arefyeva, S. Gninenko, D. Gorbunov, and D. Kirpichnikov, arXiv:2204.03984.
[105] B. Döbrich, J. Jaeckel, F. Kahlhoefer, A. Ringwald, and K. Schmidt-Hoberg, J. High Energy Phys. 02 (2016) 018.
[106] E. Byckling and K. Kajantie, *Particle Kinematics* (University of Jyvaskyla, Jyvaskyla, Finland, 1971).
[107] Y.-S. Liu and G. A. Miller, Phys. Rev. D **96**, 016004 (2017).